An empirical evaluation of functional alignment using inter-subject decoding

Thomas Bazeille, Elizabeth Dupre, Jean-Baptiste Poline, Bertrand Thirion

An empirical evaluation of functional alignment using inter-subject decoding

Thomas Bazeille[1,†,*] Elizabeth DuPre[2,†], Jean-Baptiste Poline[2], Bertrand Thirion[1]
[1] *Université Paris-Saclay, Inria, CEA, Palaiseau, 91120, France*
[2] *Montréal Neurological Institute, McGill University, Montréal, Canada*
† *These authors contributed equally to this work.*

Inter-individual variability in the functional organization of the brain presents a major obstacle to identifying generalizable neural coding principles. Functional alignment—a class of methods that matches subjects' neural signals based on their functional similarity—is a promising strategy for addressing this variability. At present, however, a range of functional alignment methods have been proposed and their relative performance is still unclear. In this work, we benchmark five functional alignment methods for inter-subject decoding on four publicly available datasets. Specifically, we consider piecewise Procrustes, searchlight Procrustes, piecewise Optimal Transport, Shared Response Modelling (SRM), and intra-subject alignment; as well as associated methodological choices such as ROI definition. We find that functional alignment generally improves inter-subject decoding accuracy though the best performing method depends on the research context. Specifically, SRM performs best within a region-of-interest while piecewise Optimal Transport performs best at a whole-brain scale. We also benchmark the computational efficiency of each of the surveyed methods, providing insight into their usability and scalability. Taking inter-subject decoding accuracy as a quantification of inter-subject similarity, our results support the use of functional alignment to improve inter-subject comparisons in the face of variable structure-function organization. We provide open implementations of the methods used.

Keywords: fMRI; functional alignment; predictive modeling; inter-subject variability

1. Introduction

A core challenge for cognitive neuroscience is to find similarity across neural diversity (Churchland 1998); that is, to find shared or similar neural processes supporting the diversity of individual cognitive experience. Anatomical variability and limited structure-function correspondence across cortex (Paquola et al. 2019, Rodriguez-Vazquez et al. 2019) make this goal challenging (Rademacher et al. 1993, Thirion et al. 2006). Even after state-of-the-art anatomical normalization to a standard space, we still observe differences in individual-level functional activation patterns that hinder cross-subject comparisons (Langs et al. 2010, Sabuncu et al. 2010). With standard processing pipelines, it is therefore difficult to disentangle whether individuals are engaging in idiosyncratic cognitive experience *or* if they are engaging in shared functional states that are differently encoded in the supporting cortical anatomy.

To address this challenge, *functional alignment* is an increasingly popular family of methods for functional magnetic resonance imaging (fMRI) analysis: from the initial introduction of hyperalignment in Haxby et al. 2011, the range of associated methods has grown to include shared response modelling (SRM; Chen et al. 2015) and Optimal Transport (Bazeille et al. 2019) with many variations thereof (see e.g. Xu et al. 2018, Yousefnezhad and Zhang 2017, among others). The conceptual shift from anatomically-based to functionally-driven alignment has opened new avenues for exploring neural similarity and diversity. In particular, by aligning activation patterns in a high-dimensional functional space (i.e., where each dimension corresponds to a voxel), we can discover shared representations that show similar trajectories in functional space but rely on unique combinations of voxels across subjects. For a review of current applications in the literature, see Haxby et al. 2020.

Nonetheless, it remains unclear how researchers should choose among the available functional alignment methods for a given research application. We therefore aimed to benchmark performance of existing functional alignment methods on several publicly accessible fMRI datasets, with the goal of systematically evaluating their usage for a range of research questions. We consider performance to include both (1) improving inter-subject similarity while retaining individual signal structure as well as (2) computational efficiency, as the latter is an important consideration for scientists who may not have access to specialized hardware. Technically up-to-date and efficient implementations to reproduce these results are provided at https://github.com/neurodatascience/fmralign-benchmark.

1.1. Defining levels of analysis: region-of-interest or whole-brain

Functionally aligning whole-brain response patterns at a voxelwise level is computationally prohibitive and may yield biologically implausible transformations (e.g., aligning contralateral regions). Therefore, currently available functional alignment methods generally define transformations within a sub-region. This constraint acts as a form of regularization, considering local inter-subject variability rather than global changes such as large-scale

* Correspondence should be addressed to: thomas.bazeille@inria.fr

functional reorganization. It also divides the computationally intractable problem of matching the whole-brain into smaller, more tractable sub-problems.

An important consideration, then, is how to define a local neighborhood. Broadly, two main strategies exist: (1) within a given region of interest (ROI) that reflects prior expectations on the predictive pattern or (2) grouping or parcellating voxels into a collection of subregions across the whole-brain. Existing functional alignment methods have been proposed at each of these scales. For example, the initial introduction of hyperalignment in Haxby et al. 2011 was evaluated within a ventral temporal cortex ROI and was later extended to aggregate many local alignments into larger transforms using a *Searchlight* scheme (Guntupalli et al. 2016). Other methods such as Optimal Transport have been evaluated on whole-brain parcellations (Bazeille et al. 2019), where transforms are derived for each parcel in parallel and then aggregated into a single whole-brain transform. Throughout this work, we therefore consider functional alignment methods at both the ROI and parcellated whole-brain level of analysis.

1.2. Quantifying the accuracy of functional alignment

1.2.1. Image-based statistics

A key question is how to objectively measure the performance of functional alignment. One approach is to consider alignment as a reconstruction problem, where we aim to reconstruct images from training data using functional alignment. These functionally aligned maps can then be compared with held-out ground-truth maps. We can quantify this comparison using image-based statistics such as the correlation of voxel activity profiles across tasks (Guntupalli et al. 2016, Jiahui et al. 2020), spatial correlation or Dice coefficient between estimated and held-out brain maps (Langs et al. 2014) or other metrics such as *reconstruction ratio* (Bazeille et al. 2019). However, these image-based statistics are sensitive to low-level image characteristics (e.g., smoothness, scaling), and their values can therefore reflect trivial image processing effects (such as the smoothness introduced by resampling routines) rather than meaningful activity patterns.

1.2.2. Adopting a predictive framework to quantify alignment accuracy

Rather than using image-based statistics, an alternative approach is to test functional alignment accuracy in a predictive framework. Prior work adopting this framework has used tests such as time-segment matching from held-out naturalistic data (e.g., Chen et al. 2015, Guntupalli et al. 2016). However, because time-segment matching relies on the same stimulus class to train and test the alignment, it is unclear whether the learnt functional transformations extend to other, unrelated tasks—particularly tasks with lower inter-subject correlation (Nastase et al. 2019). We are therefore specifically interested in predictive frameworks that probe model validity by measuring accuracy on held-out data from a different stimulus class, with or without functional realignment.

Inter-subject decoding is a well-known problem in the literature aimed at uncovering generalizable neural coding principles. Specifically, in inter-subject decoding we learn a predictive model on a set of subjects and then test that model on held-out subjects, measuring the extent to which learned representations generalize across individuals. In an information-mapping framework (Kriegeskorte and Diedrichsen 2019), decoding allows us to assess the mutual information between task conditions. Functional alignment, therefore, should facilitate information-mapping by increasing the similarity of condition-specific representations across subjects, thus improving their decoding.

Although the link between mutual information and decoding accuracy is non-trivial (Olivetti et al. 2011), we consider that measuring alignment with decoding accuracy on unseen subjects better fulfils neuroscientists' expectations of inter-subject alignment in two main ways. First, decoding accuracy provides a more interpretable assessment of performance than other measures such as mutual information estimates. Second, decoding accuracy on a held-out sample provides insight into the external validity and therefore generalizability of derived neural coding principles. Compared to image-based measures, decoding accuracy is thus a more rigorous measure of whether functional alignment improves the similarity of brain signals across subjects while also preserving their structure and usability for broader research use cases. In this work, we therefore quantify functional alignment accuracy by assessing improvements in inter-subject decoding when using functional alignment over and above anatomical alignment.

1.3. The present study

Using this inter-subject decoding framework, we: (1) establish that functional alignment improves decoding accuracy above anatomical-only alignment, (2) investigate the impact of common methodological choices such as whether alignment is learned in subregions across the whole brain or in pre-defined region-of-interest (ROI), and (3) compare the impact of specific alignment methods in whole-brain and ROI-based settings. We then provide a qualitative comparison of the transformations learnt by each method to "open the black box" and provide insights into how potential accuracy gains are achieved. Finally, we discuss the availability, usability and scalability of current implementations for each of the methods considered.

2. Materials and Methods

In this section, we first consider frameworks for aggregating local functional alignment transformations into a

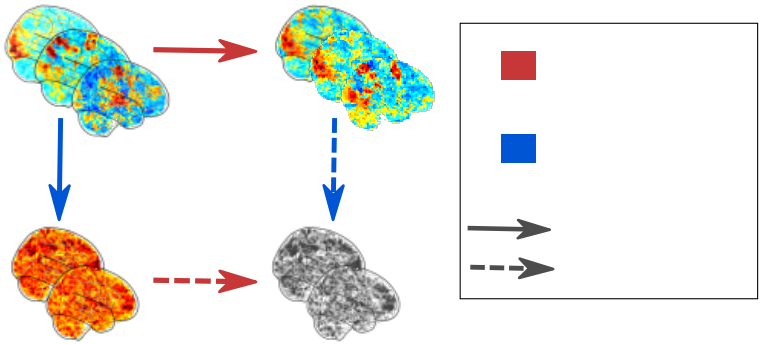

FIG. 1. **Principle of functional alignment** The goal of functional alignment is to learn correspondence between data drawn from two subjects: from a **source** subject to a **target** subject using their synchronized **alignment** data $\mathbf{A}$. In this paper, each subject comes with additional **decoding** task data $\mathbf{D}$. Red arrows describe functional alignment methods where correspondence is learnt from $\mathbf{A}^{source}$ to $\mathbf{A}^{target}$, while blue arrow describes intra-subject alignment method, where we learn correlation structure from $\mathbf{A}^{source}$ to $\mathbf{D}^{source}$. Solid arrows indicate a transformation learnt during training. Dashed arrows indicate when the previously learnt transformation is applied in prediction to estimate $\hat{\mathbf{D}}^{target}$.

single, larger transform (Section 2.1.1) that can be applied at a region-of-interest (ROI) or whole-brain scale. We proceed by introducing mathematical notations for functional alignment, then use these notations to discuss the five functional alignment methods included in our benchmark (Section 2.2). We next describe our procedure to quantify alignment performance using inter-subject decoding (Section 2.3) and a series of experiments aimed at investigating the impact of functional alignment on decoding accuracy (Section 2.4). Finally, we describe the datasets used to run each experiment (Section 2.5) and the implementations used (Section 2.6).

2.1. Aggregating local alignments

2.1.1. Comparing searchlight and piecewise schemes

As discussed in Section 1.1, alignment methods are closely linked with the definition of local correspondence models. To align the entire cortex across subjects, two main frameworks have been proposed: searchlight and piecewise analysis. Each of these frameworks use functional alignment methods to learn local transformations and aggregate them into a single large-scale alignment; however, searchlight and piecewise differ in how they aggregate transforms, as illustrated in Figure 2. The *searchlight* scheme (Kriegeskorte et al. 2006), popular in brain imaging (Guntupalli et al. 2018, 2016), has been used as a way to divide the cortex into small overlapping spheres of a fixed radius. A local transform can then be learnt in each sphere and the full alignment is obtained by averaging across overlapping transforms. Importantly, the aggregated transformation produced is no longer guaranteed to bear the type of regularity (e.g orthogonality, isometry, or diffeomorphicity) enforced during the local neighborhood fit.

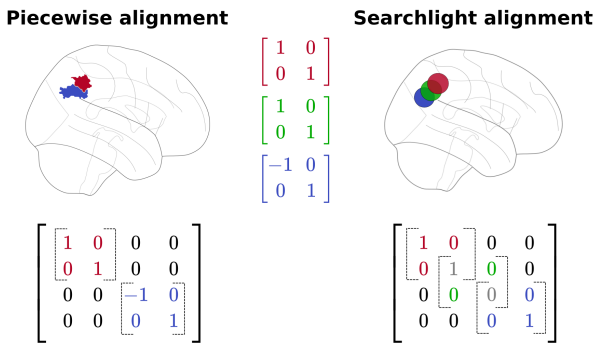

FIG. 2. **Comparing piecewise and searchlight alignment.** In this illustration, transformations are derived for the blue, green, and red areas separately. Note that the piecewise alignment does not include a green area, as this corresponds to a searchlight overlapping both the red and blue areas. For non-overlapping parcels, these transformations are stacked into a larger orthogonal matrix. For the overlapping searchlight, these transformations are aggregated, with overlapping values averaged. Note that the final transformation for the searchlight alignment is no longer orthogonal in this example.

An alternative scheme, *piecewise alignment* (Bazeille et al. 2019), uses non-overlapping neighborhoods either learnt from the data using a parcellation method—such as k-means—or derived from an *a priori* functional atlas. Local transforms are derived in each neighborhood and concatenated to yield a single large-scale transformation. Unlike searchlight, this returns a transformation matrix with the desired regularities. This framework might induce staircase effects or other functionally-irrelevant discontinuities in the final transformation due to the underlying boundaries.

2.1.2. *Aggregation schemes used in this benchmark*

In the literature to date, searchlight and piecewise aggregation schemes have both been used in conjunction with Generalized Procrustes Analysis (detailed in section 2.2) under the names hyperalignment (Guntupalli et al. 2016) and scaled orthogonal alignment (Bazeille et al. 2019), respectively. We therefore include both searchlight Procrustes and piecewise Procrustes in our benchmark. With the exception of SRM—which includes an internal regularization and can therefore be applied directly to the ROI or whole-brain data—every other local method is regularized through piecewise alignment.

As piecewise alignment is learnt within a parcellation, an important question is: which brain atlas should be used for piecewise alignment? In Section S4 we compare results from the Schaefer et al. 2018 atlases to those from parcellations derived directly on the alignment data. By default, the results presented below are derived with the 300 ROI parcellation of the Schaefer atlas unless noted otherwise. In the case of searchlight Procrustes, we selected searchlight parameters to match those used in Guntupalli et al. 2016 as implemented in PyMVPA (Hanke et al. 2009).

2.2. Description of the benchmarked methods

As we use inter-subject decoding to compare functional alignment methods, we can only consider methods that meet the following two criteria. First, the alignment transformations should be learnt on temporally synchronized (i.e., co-occuring) task data, or on contrasts matched across individuals. Second, the learnt transformations must be applicable as such on unseen data with a different task structure. These two criteria exclude several methods currently used in the literature such as regularized canonical correlation analysis (rCCA; Bilenko and Gallant 2016), gradient hyperalignment (Xu et al. 2018), connectivity hyperalignment (Guntupalli et al. 2018), and methods based on Laplacian embeddings (Langs et al. 2014).

Here, we consider five different alignment methods: searchlight Procrustes (Guntupalli et al. 2016, Haxby et al. 2011), piecewise Procrustes, Optimal Transport (Bazeille et al. 2019), shared response modelling (SRM; Chen et al. 2015), and intra-subject correlations across tasks (Tavor et al. 2016), here referred to as "intra-subject alignment." We provide a brief summary of these methods below.

2.2.1. *General notations*

Assume that for every subject we have alignment data $\mathbf{A} \in \mathbb{R}^{p \times n}$ and decoding task data $\mathbf{D} \in \mathbb{R}^{p \times d}$, where n is the number of alignment time points or frames, d the number of decoding task image and p is the number of voxels. The alignment and decoding task data are collected for both *source* and *target* subjects, which we denote with superscripts.

In general, functional alignment methods learn a transformation matrix $\mathbf{R} \in \mathbb{R}^{p \times p}$ that best maps functional signals from a source subject to those of a target subject. To do so, $\mathbf{R}$ can be seen as a linear mixing of *source* voxels signals such that $\mathbf{R}\mathbf{A}^{source}$ best matches $\mathbf{A}^{target}$. $\mathbf{R}$ is then applied on separate, held-out data from the source subject, $\mathbf{D}^{source}$ to estimate $\mathbf{D}^{target}$. Because we only learn an estimate of that held-out decoding task data, we denote this as $\hat{\mathbf{D}}^{target}$. Thus, $\hat{\mathbf{D}}^{target} = \mathbf{R}\mathbf{D}^{source}$.

We consider one method, intra-subject alignment, which uses the same alignment and decoding task data to learn a different transformation than the one described above. Specifically, in intra-subject alignment we are interested in learning $\mathbf{R}^{intra} \in \mathbb{R}^{n \times s}$, the "intra-subject" correlations between $\mathbf{A}^{source}$ and $\mathbf{D}^{source}$. We can then use $\mathbf{R}^{intra}$ to output $\hat{\mathbf{D}}^{target} = \mathbf{R}^{intra}\mathbf{A}^{target}$. Thus, the main distinction here is that intra-subject alignment does not learn a source-target mapping; instead, it learns a $\mathbf{A}$ to $\mathbf{D}$ mapping within-subjects. These notations are illustrated in Figure 1.

2.2.2. *Procrustes*

Generalized Procrustes analysis, known in the cognitive neuroscience literature as as *hyperalignment* (Haxby et al. 2011), searches for an orthogonal local transformation $\mathbf{R}$ to align subject-level activation patterns such that:

$$\min_{\mathbf{R}=s\mathbf{M}} ||\mathbf{R}\mathbf{A}^{source} - \mathbf{A}^{target}||_F^2, \quad s \in \mathbb{R}^+, \quad \mathbf{M} \in \mathbb{R}^{p \times p} \quad (1)$$

where p is the number of voxels in a given region, such that

$$\mathbf{M}^\intercal\mathbf{M} = \mathbf{I}_p \quad (2)$$

This transform can be seen as a rotation matrix mixing signals of voxels in $\mathbf{A}^{\mathbf{source}}$ to reconstruct the signal of voxels in $\mathbf{A}^{\mathbf{target}}$ as much as possible. As described in the Section 2.1.2, we compare two whole-brain implementations of this method: piecewise Procrustes and searchlight Procrustes, that differ in the way local transformations are aggregated.

2.2.3. *Optimal Transport*

Optimal transport—first introduced as a functional alignment method in Bazeille et al. 2019—estimates a local transformation $\mathbf{R}$ that aligns subject-level activation patterns at a minimal overall cost. Specifically, we can compute the cost of aligning two subject-level activation patterns as $\mathrm{Tr}(\mathbf{R} \cdot \mathbf{C})$, where $\mathbf{C}$ is the functional dissimilarity—or difference in activation patterns—between source and target, as measured by a pairwise functional distance matrix. Thus, for voxel i in $\mathbf{A}^{\mathbf{source}}$ and voxel j in $\mathbf{A}^{\mathbf{target}}$:

$$\mathbf{C}_{i,j}(\mathbf{A}^{source}, \mathbf{A}^{target}) = ||\mathbf{A}_i^{source} - \mathbf{A}_j^{target}|| \quad (3)$$

Importantly, the resulting matching is constrained to exhaustively map all source voxels to all target voxels, with every voxel having an equal weight. This implicitly yields an invertible and strongly constrained transform, preserving signal structure as much as possible. To allow for a more efficient estimation, we slightly relaxed this constraint with an additional entropic smoothing term. As introduced in Cuturi 2013, we can then find $\mathbf{R}$, the regularized Optimal Transport plan by finding a minimum for Equation 4 through the Sinkhorn algorithm.

$$\min_{\substack{\mathbf{R}\in{\mathbb{R}_+}^{p\times p};\\ \mathbf{R}\mathbf{1}=1/p,\ \mathbf{1}\mathbf{R}^\top=1/p}} \mathrm{Tr}(\mathbf{R}\cdot\mathbf{C}) - \epsilon\mathbf{H}(\mathbf{R}) \quad (4)$$

where $\epsilon > 0$, and the discrete entropy of the transformation $\mathbf{H}(\mathbf{R})$ is defined as:

$$\mathbf{H}(\mathbf{R}) \stackrel{\text{def.}}{=} -\sum_{i,j} \mathbf{R}_{i,j}(\log(\mathbf{R}_{i,j}) - 1) \quad (5)$$

This method differs from Procrustes analysis in that it yields a sparser mapping between source and target voxels with high functional similarity, making it less sensitive to noisy voxels on both ends. The level of sparsity is controlled by ϵ, a user-supplied hyper-parameter, which we set to 0.1 throughout our experiments. For our implementation, we rely on the `fmralign` package. Optimal transport transformations are calculated in a piecewise fashion, following Bazeille et al. 2019.

2.2.4. *Shared Response Model*

The Shared Response Model (SRM), introduced in Chen et al. 2015, differs from Procrustes analysis and Optimal Transport in that it provides a decomposition of all subjects's activity at once, rather than being performed pairwise. Specifically, SRM estimates a common shared response $\mathbf{S}$ and a per-subject orthogonal basis $\mathbf{W}^i$ from subject-level alignment data $\mathbf{A}^i$ such that:

$$\min_{\mathbf{W}^1,\dots,\mathbf{W}^n,\mathbf{S}} \sum_i ||\mathbf{A}^i - \mathbf{W}^i\mathbf{S}||_F^2 \ \ \forall\ \mathbf{i},\ \ \mathbf{S}\in\mathbb{R}^{k\times n},\ \ \mathbf{W}^i\in\mathbb{R}^{p\times k} \quad (6)$$

where n is the number of time points, p is the number of voxels, and k is a hyper-parameter indexing the dimensionality, such that:

$$\mathbf{W}^{i\intercal}\mathbf{W}^i = \mathbf{I}_k \quad (7)$$

In practice, SRM decomposes the signal of many subjects in a common basis, with the same orthogonality constraint as Procrustes. This ability to jointly fit inter-subject data through orthogonal transforms makes it reminiscent of Procrustes, with a caveat: SRM is effective if the number of components k is large enough to capture all distinct components in the signal. In this work, we set k to 50 components as in the original SRM benchmarks provided in Chen et al. (2015).

We specifically use the FastSRM implementation proposed by Richard et al. 2019 and available in the BrainIAK library (RRID: SCR_01 4824), that approximates this calculation with an emphasis on improved computational performance. For full details on the computational advantages of FastSRM, we direct the reader to their work.

2.2.5. *Intra-subject alignment*

Another alternative to pairwise functional alignment has been proposed in Tavor et al. 2016. In their paper, Tavor and colleagues show that while individual activity patterns in each task may appear idiosyncratic, correspondences learnt across different tasks using a general linear model (e.g., to predict object recognition task from movie-watching data derived features) display less across-subject variability than individual activity maps. This provides an interesting twist on the typical functional alignment workflow: while most methods learn alignments within a single task and across subjects, we can instead learn within-subject correlations across tasks. The structure of learnt task-specific correlations should then hold in new, unseen subjects. We include here a method for learning these intra-subject correlations in a piecewise fashion, which we call *intra-subject alignment*.

Figure 3 illustrates how we can learn the local-level correlation structure between two independent tasks $\mathbf{A}^{source} \in \mathbb{R}^{p\times n}, \mathbf{D}^{source} \in \mathbb{R}^{p\times d}$ within a single *source* subject. We denote the mapping between these tasks as $\mathbf{R}^{intra}$ to distinguish it from mappings which are learnt between pairs of subjects.

First, we divide alignment and decoding data into 1000 parcels using the highest-resolution Schaefer atlas (Schaefer et al. 2018). On a local parcel i, each voxel is considered a sample and we train $\mathbf{R}_i^{intra} \in \mathbb{R}^{p_i\times d}$ through ridge regression:

$$\mathbf{R}_i^{intra} = \arg\min_{\mathbf{R}_i} ||\mathbf{A}_i^{source}\mathbf{R}_i - \mathbf{D}_i^{source}||_F^2 + \alpha||\mathbf{R}_i||_F^2 \quad (8)$$

The hyperparameter α is chosen with nested cross-validation among five values scaled between 0.1 and 1000 logarithmically.

After repeating this procedure for all *source* subjects, we then use $\mathbf{R}^{intra}$ to estimate decoding data for *target* subject as $\hat{\mathbf{D}}^{target} = \mathbf{R}^{intra}\mathbf{A}^{target}$. We observed that—unlike other piecewise techniques (Section S4)—the decoding accuracy strictly improved with the number of parcels in the atlas used so we used the highest resolution atlas available. As with other functional alignment methods, we can evaluate the quality of our estimation using an inter-subject decoding framework.

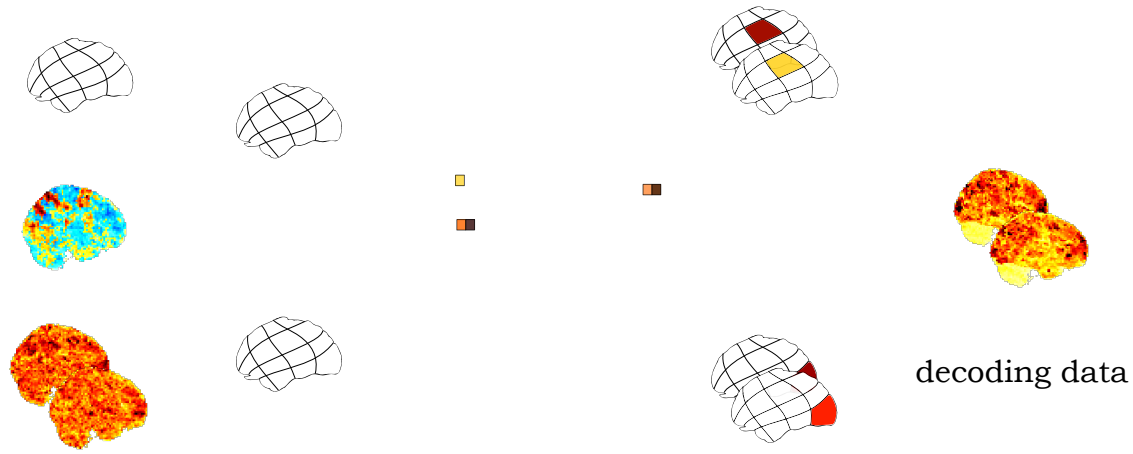

FIG. 3. **Intra-subject alignment.** Using intra-subject alignment to learn piecewise correlations between a single subject's alignment and decoding task data. As with other piecewise methods, this mapping is learnt separately for all parcels $i \ldots j$ of the chosen parcellation. For each parcel, we use cross-validated ridge regression to learn the mapping between the two task conditions—alignment data $\mathbf{A}$ and independent decoding task data $\mathbf{D}$—for this source subject. For the ith parcel, we denote this mapping as the matrix $\mathbf{R}^i$. We then aggregate these piecewise predictions into a single, whole-brain prediction $\hat{\mathbf{D}}$. In training, this prediction can be directly compared to the ground-truth decoding data, $\mathbf{D}$. When testing, we would have access to the target subject's alignment data $\mathbf{A}$ but not their decoding task data, $\mathbf{D}$.

2.3. Experimental procedure

For each dataset considered (as described in Section 2.5), we calculated the inter-subject decoding accuracy for standard, anatomical-only alignment and for each of the five considered functional alignment methods.

To calculate inter-subject decoding accuracy, we took the trial- or condition-specific beta maps generated for each dataset (see Section 2.5 for full details on beta-map generation) and fit a linear Support Vector Machine (SVM). In order to ensure fair comparisons of decoding accuracy across experiments, we chose a classifier with no feature selection and default model regularization. Classifiers were implemented in scikit-learn (Pedregosa et al. 2011), and decoding accuracy was assessed using a leave-one-subject-out cross-validation scheme. That is, the linear SVM was trained to classify condition labels on all-but-one subject and the resulting trained classifier was used without retraining on the held-out subject, providing an accuracy score for that cross-validation fold.

For each dataset, we first calculated the inter-subject decoding accuracy using standard anatomical alignment. This served as a baseline accuracy against which we could compare each functional alignment method. Using alignment data, functional alignment transformations were then learnt for each pairwise method, where the left-out subject for that cross-validation fold was the target subject for functional alignment. Inter-subject decoding accuracy was then re-calculated after applying functional alignment transformations to the decoding beta maps. In the special case of SRM—which calculates an alignment from all provided subjects in a single decomposition—we withheld the left-out subject from the shared response estimation step to avoid data leakage and finally learned its projection to the resulting shared response space, in which decoding was performed.

For each cross-validation fold, we report the inter-subject decoding accuracy of a given functional alignment method after subtracting the baseline, anatomical-only accuracy for that same fold. An overview of the experimental procedures is provided in Figure 4.

2.4. Main experiments

Experiment 1 uses the experimental procedure described previously to assess accuracy gains provided by alignment methods with respect to anatomical alignment when applied on whole-brain images. We benchmarked the five methods described in Section 2.2: piecewise Procrustes, searchlight Procrustes, piecewise Optimal Transport, SRM, and intra-subject alignment, with relevant hyperparameters selected as described previously. Results of this benchmark (on five tasks from four datasets as described in Section 2.5) are presented in Section 3.1. For each method, we also assessed its computation time relative to piecewise Procrustes alignment. Piecewise Procrustes provides a reasonable computational baseline as it is the only considered alignment method that does not include a hyperparameter and therefore shows a stable computation time across experiments.

We estimate the noise ceiling for this task as within-subject decoding accuracy. Within-subject decoding was calculated separately for each subject as the average leave-one-session-out decoding accuracy. We can then directly compare this accuracy value to the inter-subject decoding accuracy when that subject is the target—that is, the left-out—subject. The difference between within- and anatomical inter-subject decoding accuracies, then,

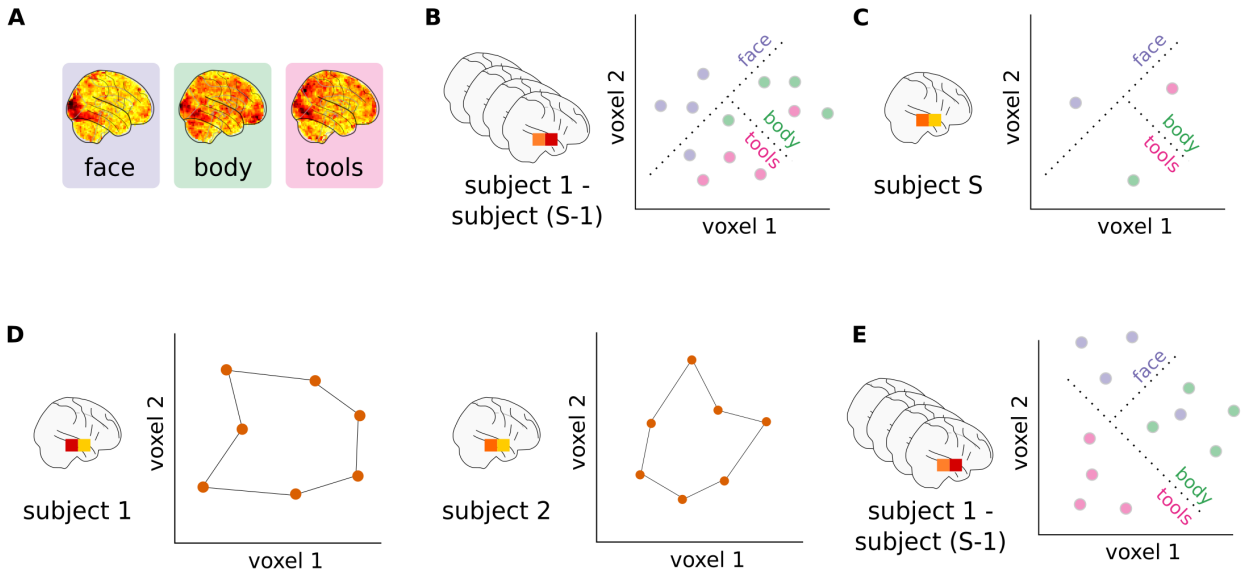

FIG. 4. **Analysis pipeline.** (A) First-level general linear models are fit for each subject to derive trial- or condition-specific beta-maps for each session. (B) These beta maps and their matching condition labels are used to train a linear SVM on the training set of subjects. (C) The trained classifier is applied on a held-out test subject, and accuracy is assessed by comparing the predicted and actual condition labels. (D) On a separate task, we compare subject-level activation patterns as trajectories in the high-dimensional voxel space. This allows us to learn functional alignment transformations that maximize the similarity of these high-dimensional spaces. (E) These voxel-wise transformations are applied on the decoding beta maps, and a new linear SVC is trained to predict condition labels. This trained classifier can then be applied to the held-out test subject and decoding accuracy assessed as in (C).

is a good approximation of the decoding accuracy lost to inter-subject variability; therefore, it provides a range of possible accuracy gains that can be expected from functional realignment.

We then conducted *Experiment 2* to understand how whole-brain results compare to ROI-based analyses. Specifically, we replicated *Experiment 1* within selected ROIs, where ROIs were chosen based on *a priori* expectations of each decoding task (see Section 2.5 for details for each dataset). Results from *Experiment 2* are shown in Section 3.2.

Experiment 3 tackles the notoriously hard problem of understanding how each of the considered methods align subjects by examining qualitatively their impact on activity patterns across individuals. To "open the black-box," we reused IBC dataset full-brain alignments learnt in *Experiment 1*. Specifically, we consider the transformation to sub-04's activity pattern from all other subjects's functional data. With these transformations, we align two contrasts from the IBC dataset: Rapid Serial Visual Presentation of words (RSVP language task) and sound listening. Finally, we run a group conjunction analysis (Heller et al. 2007) on these aligned contrasts and display its results. This statistical analysis, more sensitive than its random effect equivalent on small samples, allows one to infer that every subject activated in the region with a proportion γ showing the effect considered. Here we use $\gamma = 0.25$ to recover all regions selectively activated by at least a few subjects, and we show in Section 3.3 how this group functional topography is modified by alignment.

2.4.1. *Control analyses*

In addition to our three main experiments, we ran three additional control analyses on the IBC dataset. First, we aimed to assess the impact of the brain parcellation and its resolution on piecewise alignment by comparing whole-brain decoding accuracy for two IBC dataset tasks using piecewise Procrustes across both data-driven and pre-defined parcellations (Section S4). Second, we calculated inter-subject decoding performance after applying Gaussian smoothing kernels of several widths on both IBC dataset decoding tasks (Section S5). Gaussian smoothing is of particular interest as a comparison to functional alignment, as it is commonly used to facilitate inter-subject comparisons by smoothing over residual variance in functional mappings. Finally, in a third control experiment, we assessed the impact of whether data is represented on the surface or the volume and resolution on decoding accuracy in the IBC RSVP language task (Section S6).

Dataset	S	Alignment data	Decoding task data	Categories	d
Individual Brain Charting (IBC)	10	53 contrasts from HCP and ARCHI task batteries	RSVP Language	Words, Non-Words, Consonants, Simple / Complex sentences, Jabberwocky	360
			Sounds dataset	Voice, Nature, Animal, Music, Speech, Tools	72
BOLD5000	4	ImageNet content	Plant, Animal, Food, Artifact	Coco, Imagenet and Scenes images	350
Forrest	10	Forrest Gump audio-movie listening	Music genre	Country, Metal, Ambient, Symphonic, Rock	200
Courtois Neuromod	4	Life movie watching	Visual category	Body, Face, Place, Tools	52

TABLE I. **Datasets used to benchmark alignment methods.** The four datasets used in this benchmark, where each dataset consists of S subjects. We note the alignment data used for each dataset, showing the range of possible task structures which work for alignment—from static images for BOLD5000, to statistical contrast maps for IBC, to complex audio or audio-visual movies for Forrest and Courtois Neuromod. We also note the decoding task(s) used for each dataset. Of note, IBC dataset has two independent decoding tasks, bringing the total number of decoding tasks to five. Each subject's decoding task data comprises d images evenly divided across the listed stimulus categories (except for BOLD5000 categories which are unbalanced).

2.5. Datasets and preprocessing

In order to assess the performance of each functional alignment method in a range of applications, we searched for publicly accessible datasets that included both a task suitable to learn the alignment (e.g. naturalistic or localizer protocols) as well as an independent decoding task on which we could evaluate functional alignment performance. After discarding datasets where we could not obtain above-chance accuracy levels for within-subject decoding, we retained four datasets: BOLD5000 (Chang et al. 2019), Courtois-NeuroMod (Boyle et al. 2020), Individual Brain Charting (IBC; Pinho et al. 2018), and Study Forrest (Hanke et al. 2016). For the IBC dataset, we included both a language (RSVP language) and auditory (Sounds dataset) decoding task, yielding a total of five decoding tasks that probe visual, auditory and language systems. For a complete description of the alignment and decoding data included in each experiment, please see Table I.

BOLD5000, StudyForrest and Courtois-NeuroMod were preprocessed with fMRIPrep (Esteban et al. 2019), while IBC data were preprocessed using an SPM-based pipeline as described in Pinho et al. 2018. A complete description of the fMRIPrep preprocessing procedures is available in the appendix (Section S1). Preprocessed data were then masked using a grey matter mask, detrended, and standardized using Nilearn (Abraham et al. 2014). To reduce the computational cost of functional alignment, we downsampled all included datasets to 3mm resolution. Decoding task data were additionally smoothed with a 5mm Gaussian kernel. A general linear model (GLM) was fit to each decoding task run to derive trial-specific beta maps (or condition-specific beta maps for the Courtois Neuromod and IBC Sounds tasks), which were carried forward for inter-subject decoding.

As described in Section 2.3, *Experiment 2* uses predefined regions of interest (ROIs). We selected large, task-relevant ROIs to ensure that sufficient signal was available when decoding. A large visual region, extracted from the Yeo7 (Buckner et al. 2011) atlas was used for the visual tasks in BOLD5000 and Courtois-NeuroMod. For Forrest and IBC Sounds—which are auditory tasks—we took the Neuroquery (Dockès et al. 2020) predicted response to the term "auditory". We then compared this predicted response with the BASC atlas (at scale 36; Bellec et al. 2010) and took the parcel most overlapping with the predicted response; namely, parcel 25. For IBC RSVP, which is a reading task, we extracted the BASC (at scale 20) atlas components most overlapping with MSDL (Varoquaux et al. 2011) atlas parcels labeled as left superior temporal sulcus, Broca and left temporo-parietal junction: namely, the 8 and 18 BASC components. We then kept only the largest connected component. All included ROIs are displayed in Figure 7.

2.6. Implementation

With the exception of Courtois Neuromod, all other included datasets are available on OpenNeuro (Poldrack et al. 2013) under the following identifiers: *ds000113* (Study Forrest), *ds001499* (BOLD5000), and *ds002685* (IBC). Courtois Neuromod `2020-alpha2` release will be available under a data usage agreement as outlined on https://docs.cneuromod.ca.

Our pipeline entirely relies on open-source Python software, particularly the SciPy stack (Virtanen et al. 2020). All included methods are implemented in `fmralign` or accessed through their original, open source implementations as described in Section 2.2. To ease replication and extension of the presented results, we have created the `fmralign-benchmark` repository under https://github.com/neurodatascience/fmralign-benchmark. This repository provides an implementation of the procedures adopted in these experiments, building on `fmralign` and previously cited tools.

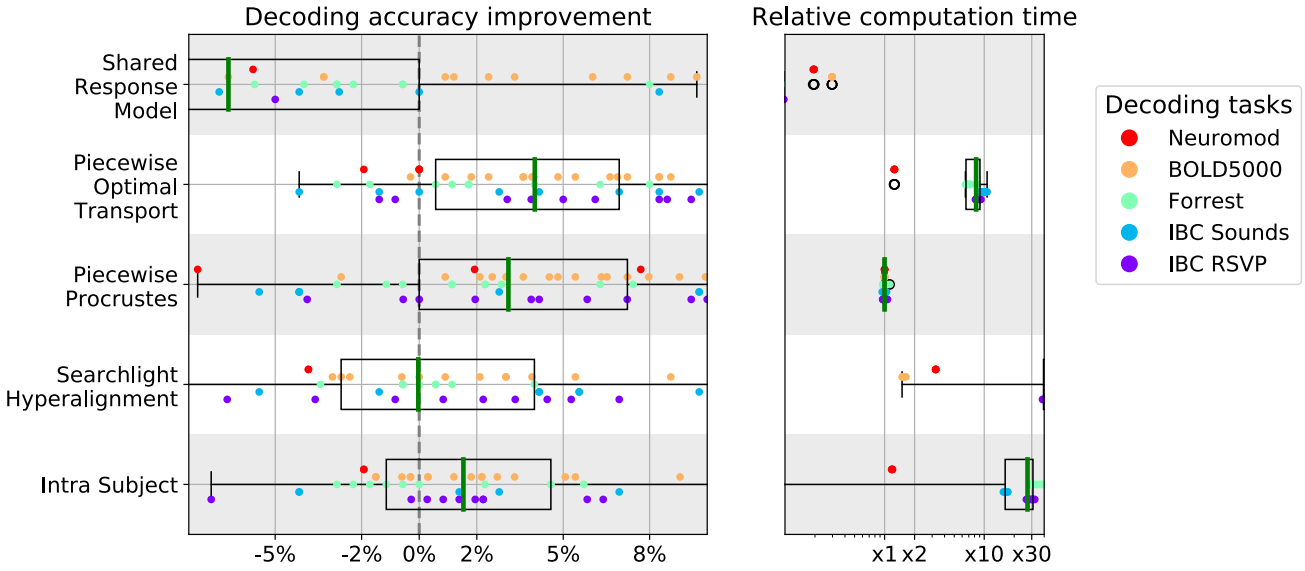

FIG. 5. **Decoding accuracy improvement and computation time after whole-brain functional alignment.** In the *left panel*, we show decoding accuracy improvement for each of the considered functional alignment methods at the whole-brain level of analysis. Each dot represents a single subject, and subjects are colored according to their decoding task. To aggregate results across datasets, we show accuracy scores after subtracting inter-subject decoding accuracy for the same leave-one-subject-out cross-validation fold with anatomical-only alignment. In the *right panel*, we show the computational time for each of the considered methods. All computation times are depicted as relative to piecewise Procrustes. For both panels, each box plot describes the distribution of values across datasets, where the green line indicates the median. We see that piecewise Procrustes, Optimal Transport, and intra-subject alignment consistently improve decoding accuracy across datasets. We also see that piecewise Optimal Transport is 10 times slower and searchlight Procrustes is more than 30 times slower than piecewise Procrustes.

3. Results

3.1. Functional alignment improves inter-subject decoding

The *left panel* of Figure 5 displays absolute decoding accuracy change brought by each functional alignment method relative to anatomical alignment on whole-brain images. As every method is trained and tested on same cross-validation folds, we report the fold-by-fold performance change. The *right panel* displays each method's relative computation time compared to piecewise Procrustes alignment. For each panel, each point displayed is the result for one leave-one-subject-out cross validation fold and each color corresponds to one of the five decoding tasks. Note that these timings are based on available implementations — `fmralign` for piecewise alignment methods, `pymvpa2` for searchlight, and `BrainIAK` for SRM— and are therefore subject to change as implementations improve. Nonetheless, these estimates provide insight into the current state-of-the-art.

3.1.1. Alignment substantially improves inter-subject decoding accuracy

Overall, we can conclude that most functional alignment methods consistently improve decoding accuracy with gains from 2-5% over baseline. This trend is relatively consistent across datasets and target subjects. Thus, alignment methods manage to reliably reduce individual signal variability while preserving task-relevant information in a variety of conditions. Although between-dataset variance yields large boxplot, these methods have significant effect. Indeed, as reported in Table S1, baseline accuracy is around 20% above chance across datasets. In this setting, a 5% average improvement across datasets is a substantial increase.

In order to further contextualize these results, we also estimated the noise ceiling for inter-subject decoding. Figure 6 reports that across datasets, the leave-one-session-out (i.e., within-subject) decoding accuracy for the target subject is on average 8.5% higher than the corresponding leave-one-subject-out (i.e., inter-subject) decoding accuracy after standard anatomical alignment for the same target subject. Thus, we expect that functional alignment methods will achieve at most an 8.5% increase in inter-subject decoding accuracy over standard, anatomically-driven alignment. In this light, we can see that the best functional alignment method recovers roughly half of the decoding accuracy lost to inter-subject variability.

Additional control analyses suggest that this effect cannot be explained by smoothing (Section S5). We further find that the presented results are largely insensitive both

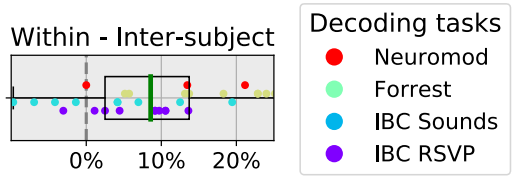

FIG. 6. **Within-subject minus inter-subject decoding accuracy.** We show the difference between the average leave-one-session-out within-subject decoding accuracy and anatomically-aligned leave-one-subject-out inter-subject decoding accuracy, when that target subject is left-out. Thus, each dot corresponds to a single subject, and the dot's color indicates the decoding task. Of note, BOLD5000 was dropped since it didn't contain inter-subject decoding cross-validation didn't have independent folds therefore could not be used for within-subject cross-validation. The box plot describes the distribution of differences, where the green line represents the median value. We that argue this difference approximates the effects of inter-individual variability, and so the best average accuracy improvement we can hope for using functional alignment is around 9%.

to whether the data is represented on the cortical surface or in volumetric space as well as to the parcellation resolution used (see section S6).

3.1.2. Piecewise methods show computational and accuracy advantages

Procrustes alignment results in better inter-subject decoding accuracies when performed in a piecewise as compared to a searchlight approach. Specifically, searchlight shows very low decoding accuracies on average, suggesting that its internal averaging destroys part of the signal structure recovered by Procrustes. With respect to computational cost, we can see that searchlight Procrustes is 30 times slower on average than piecewise Procrustes. These results suggest that piecewise alignment is a better choice when calculating functional alignment transformations on full-brain data. Moreover, Section S4 shows that gains to expect from piecewise alignment are quite insensitive to the resolution and type of parcellation used; i.e., taken from an atlas or learnt from subject data.

Another piecewise method, Optimal Transport, yields the highest decoding accuracy on average. Compared to other methods—especially Procrustes—we observe that Optimal Transport gives non-trivial gains in most configurations and only rarely decreases decoding accuracy, likely because of the stronger constraints that it imposes. However, this extra-performance comes at a computational cost: it is on average 10 times slower than Procrustes.

3.1.3. Task-specific mappings can be learnt within subjects

The intra-subject alignment approach differs from other considered functional alignment methods in that it learns mappings between the alignment data and decoding task data, with the assumption that these mappings can be generalized across subjects. Our results support this assumption, although this method yields gains half as large as the best performing alignment method and comes with a significant computational cost. Part of this cost can be accounted for by the increase in the number of parcels which must be learnt to preserve signal specificity. Nonetheless, using task-specific mappings as a functional alignment method suggests that future work on refining related methods may be a promising direction of research.

3.2. Whole-brain alignment outperforms ROI-based alignment

The *left panel* of Figure 7 displays the performance of each functional alignment method relative to anatomical alignment within task-relevant ROIs. The *right panel* displays each method's relative computation time compared to piecewise Procrustes alignment.

When visually compared to Figure 5, ROI-based decoding accuracies appear to be slightly lower than whole-brain decoding accuracies for most of the considered methods. We directly compare ROI-based and whole-brain alignment in a supplementary analysis, depicted in Figure S1, confirming that ROI-based decoding accuracies are in fact lower. Our results support previous work from the inter-subject decoding literature (Chang et al. 2015, Schrouff et al. 2018) and suggest that full-brain piecewise alignment yields the best overall decoding pipeline.

Computationally, we see that piecewise Optimal Transport shows faster performance when restricting the alignment to an ROI, running nearly as quickly as piecewise Procrustes. The slowest methods here are around 10 times slower than piecewise Procrustes and 50 times slower than SRM.

We also note that—on average—intra-subject alignment does not show increased inter-subject decoding accuracy within task-relevant ROIs. We suspect that this is likely because the very low number of components predicted do not enable it to find stable multivariate patterns in this context.

3.2.1. SRM shows higher performance in ROI-based decoding

Uniquely, the Shared Response Model (SRM) shows decreased whole-brain decoding accuracy compared to ROI-based decoding accuracy. Specifically, as visible in Figure 7, SRM yields the best accuracy improvement at the ROI level of analysis at a low computational cost (five times quicker than piecewise Procrustes). In ROI-based setting, the baseline is around 10 % above chance in all datasets (except Neuromod). Hence SRM 3% accuracy increase is a strong effect(see Table S2).

SRM is not well-suited to full-brain decoding because

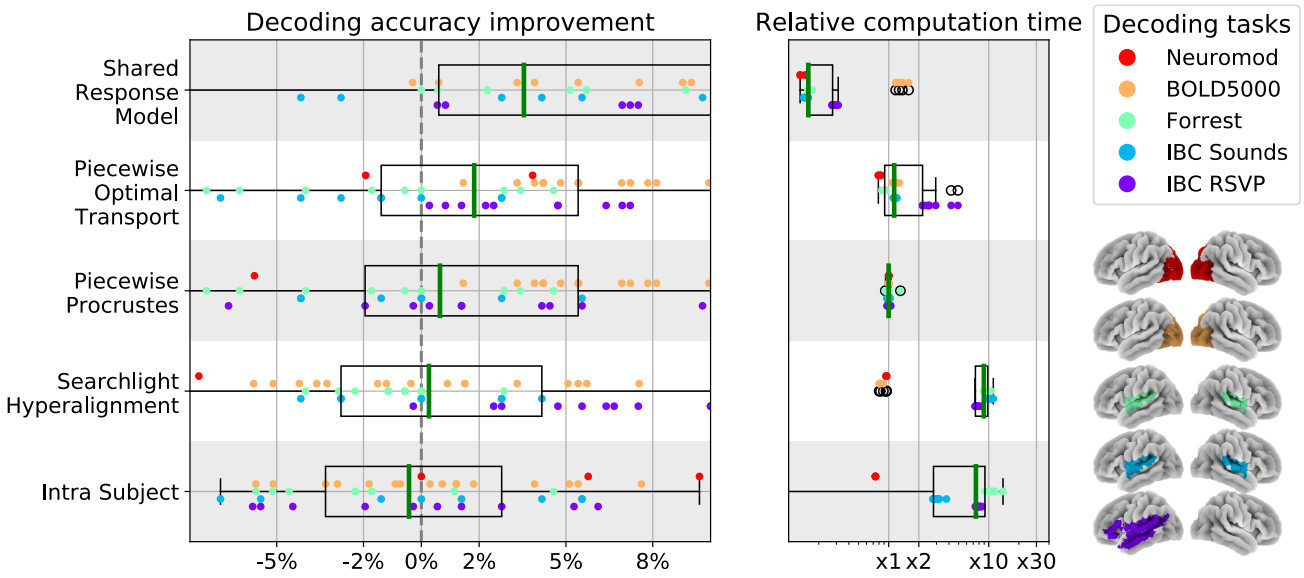

FIG. 7. **Decoding accuracy improvement and computation time after ROI-based functional alignment.** In the *left panel*, we show decoding accuracy for each of the considered functional alignment methods at the ROI level of analysis. The ROIs used for each dataset are displayed on the *far right*. Each dot represents a single subject, and subjects are colored according to their decoding task. Rather than raw values, we show accuracy scores after subtracting inter-subject decoding accuracy for the same leave-one-subject-out cross-validation fold with anatomical-only alignment. In the *right panel*, we show the computational time for each of the considered methods. All computation times are depicted as relative to piecewise Procrustes. For both panels, each box plot describes the distribution of values where the green line indicates the median.

it estimates the *shared response* using a limited number of components. Projection into a common space results in sharp data rank reduction and thus a loss of information compared to using original data. In an ROI, by contrast, we have a smaller number of voxels p compared to the number of training samples n. This increases the ratio of n/p which ensures both (1) more stable estimations thanks to increased number of samples (2) that we do not lose relevant information when projecting voxel signal to a lower number of components; i.e., the *shared response* (n/p must be above 1 to ensure full-rank decomposition).

3.3. Qualitative display of transformations learnt by various methods

Understanding the effects of high-dimensional transformations—such as those used in functional alignment—is non-trivial. To aid in this process, we "open the black box" by functionally aligning a group of subjects to an individual target subject's functional space and depict the resulting maps in Figure 8. Here, we reuse whole-brain alignments learnt in *Experiment 1*.

We also display the ground-truth individual activation maps in *panel A*, in order to better highlight how each method affects the signal distribution. As a reminder, the contrast data displayed here was not used to learn alignments, so it means that alignment learnt on various task data, not specifically related to language nor audition carried enough information for fine-grain registration of these networks.

We can see that overall, functional alignment methods enhance group-level contrasts compared to anatomical-only alignment; i.e., activation maps are more similar across functionally-aligned subjects. This result is not at the expense of signal specificity, since the aligned group topographies are still sharp. From the comparison between panels *A* and *B*, we can also conclude that alignment methods bring group topography much closer to the targeted subject topography across many contrasts. Nonetheless, we can still observe that there seems to be a trade-off between sharpness of activation (low smoothness of image, due to low variance across aligned subjects) with Optimal Transport, and accuracy of their location compared to the target ones (low bias introduced by the matching) with searchlight Procrustes.

One exception to this is the Shared Response Model (SRM), that yields smoother group topography than the other alignment methods considered. This discrepancy can be explained by the fact all of the depicted alignments are learnt on full-brain data. For SRM, this truncates the whole-brain signal to its main components, and the visual smoothness impression is thus a correlate of its poor performance in full-brain decoding.

4. Discussion

In this work, we have proposed a new procedure to measure the information recovered through functional

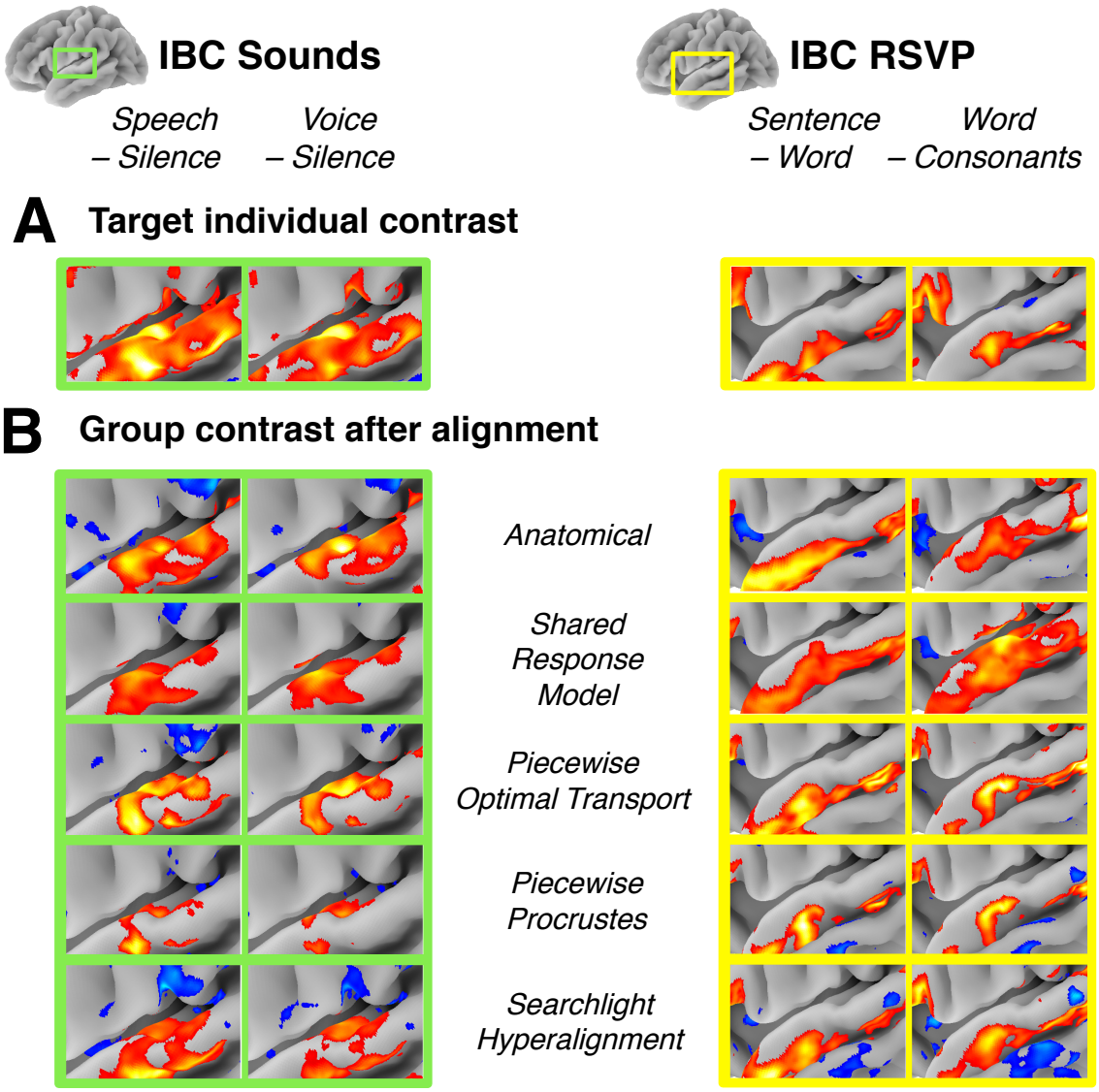

FIG. 8. **Comparison of alignment methods geometrical effects.** (A) Activation patterns for the Target subject (IBC sub-04) for two contrasts from the IBC Sounds task (*Speech* > *Silence, Voice* > *Silence*) and IBC RSVP task (*Sentence* > *Word, Word* > *Consonants*). Here, we only show contrast maps from a sub-region of the temporal-parietal region containing contrast-relevant information. Note that this sub-region differs slightly between the Sounds and RSVP task. (B) Visualization of a group conjunction analysis of all IBC subjects after alignment to the target subject for each of the considered methods. We used a γ value of 0.25 in the group conjunction analysis, which corresponds to at least 25% of the IBC sample showing activation in this temporal-parietal region after alignment. For ease of comparison, the colorbar for each contrast and method was scaled to show the full range of values (i.e., the colorbar spans different interval across methods and contrasts) and so is not included here. All displayed maps were thresholded at 1/3 of their maximum value. We see that functional alignment yields stronger contrasts overall when compared to anatomical alignment. Piecewise Procrustes and piecewise Optimal Transport yield less smooth representations, better preserving signal specificity.

alignment using inter-subject decoding, and we have used this framework to benchmark five functional alignment methods on five distinct decoding tasks across four publicly available datasets.

In general, we find that functional alignment improves inter-subject decoding accuracy in both whole-brain and ROI settings. These results, combined with our qualitative visualization of the effects of functional alignment on signal structure, suggest that functional alignment improves inter-subject correspondence while matching signal to realistic functional topographies. This extend conclusions from earlier work (Güçlü and van Gerven 2015, Guntupalli et al. 2016). Specifically, the baseline inter-subject decoding accuracy is roughly 20% above chance

across datasets (Table S1). The best performing method in our benchmark, piecewise Optimal Transport bring a substantial 4% improvement over this baseline on average, recovering roughly half of the accuracy lost to inter-subject variability.

Although we see improved decoding accuracy on average, we also note that the functional alignment methods considered show different performance at the ROI and whole-brain scale. While piecewise Optimal Transport performs best when aggregating transformations across the whole-brain, SRM performs best to enhance decoding within regions of interest, bringing a 3% important improvement over a baseline only 10-15% above chance (Table S2). We therefore caution that the most appropriate method may depend on the research question of interest. Nonetheless, we observe that increases in decoding accuracy were reliably greater than the effect of Gaussian smoothing (see section S5). From a minimalistic replication, this effect seem to hold for both volumetric and surface data, and at different parcellation resolutions (see section S6; cf. Oosterhof et al. 2011).

Our benchmark also brings new evidence that the latent correspondences that can be learnt between different tasks display less inter-individual variability than the task-specific activation maps (Tavor et al. 2016). *Experiment 1* indeed showed that such correspondences could even be used to transfer signals subjects to solve an inter-subject decoding problem, which is—to the best of our knowledge—an original experimental result. By releasing efficient and accessible implementations of these methods in the `fmralign` package, we hope to facilitate future cognitive neuroscience research using functional alignment methods.

4.1. Combining local alignment models

Across datasets, we find that the spatial framework of alignment and decoding significantly affects subsequent performance. Notably, piecewise Procrustes outperforms searchlight Procrustes, both in terms of accuracy and computational performance. The methodological difference between these methods is whether alignment transformations are learnt within overlapping neighborhoods (as in searchlight Procrustes) or not (as in piecewise Procrustes). Searchlight alignment suffers in that the overlap between searchlights requires multiple computations for a given neighborhood, and the aggregated transformation is no longer guaranteed to reflect properties of the original transforms, e.g. orthogonality. Although piecewise alignment may introduce discontinuities at parcel boundaries, in our results this overall benefited decoding performance. Importantly, we found that the improved performance of piecewise Procrustes was largely insensitive to parcel size and definition (see Figure S2).

SRM performance was found to depend strongly on the spatial context, though at a larger scale than local neighborhood definition. Specifically, SRM performs best when restricted to an ROI. This can be explained by the built-in dimensionality reduction that may discard relevant information when applied at a whole-brain level of analysis. We therefore suggest that an extension of SRM to piecewise alignment may be an important direction for future research.

4.2. Evaluating alignment performance with decoding

We use inter-subject decoding to quantify the amount of mutual information recovered by functional alignment methods. In general, identifying publicly available datasets with tasks appropriate for both inter-subject decoding as well as functional alignment remains a challenge. Beyond the four datasets included in these results, we investigated several other publicly available datasets such as the Neuroimaging Analysis Replication and Prediction Study (NARPS; Botvinik-Nezer et al. 2020),the Healthy Brain Network Serial Scanning Initiative (HBN-SSI; O'Connor et al. 2017), the interTVA dataset (Aglieri et al. 2019, available as Openneuro *ds001771*) and the The Dual Mechanisms of Cognitive Control Project (DMCC, Braver et al. 2020).

We had difficulties in achieving sufficient baseline accuracy levels in these and other datasets, and we therefore chose not to include them in the present study. This suggests that the amount of signal discriminating complex experimental conditions is not strong enough to find inter-subject patterns robust to variability in many publicly available datasets, likely due to limited sample sizes and inappropriate experimental designs. We hope that broader recognition of the benefits of using inter-subject decoding to uncover neural coding principles across subjects—using functional alignment if necessary—will encourage investigators to collect and share more datasets supporting this type of analysis. Greater data availability will encourage robust, principled comparisons of alignment methods and foster progress in the field.

4.3. Study limitations and future directions

Although our study provides a broad evaluation of the performance of several functional alignment methods, there are several dimensions which we hope future work will better address. Notably, we did not thoroughly investigate how alignment performance is impacted by image resolution and whether data are represented on the surface or the volume. Using volumetric images downsampled to a standard resolution of 3mm isotropic enabled us to make fairer comparisons across datasets at a reasonable computational cost. We also show in Section S6 that results from piecewise Procrustes alignment on the IBC dataset hold in a higher resolution, surface-based setting. Nonetheless, other functional alignment methods might show different patterns of performance in this setting or at different resolution levels. Moreover, applying these methods on high-resolution images

is an exciting perspective to better understand how precise brain function varies across subjects. To progress in this direction, a stronger focus on developing computationally efficient methods will be needed. The use of high-resolution parcellations—combined with more efficient implementations of piecewise Optimal Transport or a piecewise Shared Response Model—seem to be particularly promising directions.

We have also not examined the impact of alignment data on the learnt transformations and whether this impact varies across cortex. That is, we could further ask whether certain kinds of stimuli may produce more accurate functional alignments for specialized functional regions. In general, the surveyed functional alignment methods view each subject alignment image as a sample, and the resulting transformation is trained to match corresponding samples across subjects. If some training images lack stable signal in a given ROI, functional alignment methods are unlikely to learn meaningful transformations in this region. In future work, we intend to address the above questions to learn more about when functional alignment methods are most appropriate.

5. Conclusion

In the present work, we have provided an extensive benchmark of five popular functional alignment methods across five unique experimental tasks from four publicly available datasets. Assessing each method in an inter-subject decoding framework, we show that Shared Response Modelling (SRM) performs best at a region-of-interest level of analysis, while Optimal Transport outperforms other methods at the whole-brain scale. Our results support previous work proposing functional alignment to improve across-subject comparisons, while providing nuance that some alignment methods may be most appropriate for a given research question. We further suggest that identified improvements in inter-subject decoding demonstrate the potential of functional alignment to identify generalizable neural coding principles across subjects.

Acknowledgments

This project has received funding from the European Union's Horizon 2020 Framework Programme for Research and Innovation under the Specific Grant Agreement No. 945539 (Human Brain Project SGA3) and the Digiteo French program. This work was also partially funded by the National Institutes of Health (NIH) NIH-NIBIB P41 EB019936 (ReproNim) NIH-NIMH R01 MH083320 (CANDIShare) and NIH RF1 MH120021 (NIDM), the National Institute Of Mental Health under Award Number R01MH096906 (Neurosynth), as well as the Canada First Research Excellence Fund, awarded to McGill University for the Healthy Brains for Healthy Lives initiative and the Brain Canada Foundation with support from Health Canada.

We wish to thank all researchers that made this study possible by making their datasets publicly available, especially J. Etzel, S. Takerkart, and P. Bellec for kindly taking the time to provide us preprocessed version of their datasets and thorough explanations of their experimental designs. Data from the Courtois project on neural modelling was made possible by a generous donation from the Courtois foundation, administered by the Fondation Institut Gériatrie Montréal at CIUSSS du Centre-Sud-de-l'île-de-Montréal and University of Montreal. The Courtois NeuroMod team is based at Centre de Recherce de l'Institut Universitaire de Gériatrie de Montréal, with several other institutions involved. See the cneuromod documentation for an up-to-date list of contributors (https://docs.cneuromod.ca).

Abraham, A., Pedregosa, F., Eickenberg, M., Gervais, P., Mueller, A., Kossaifi, J., Gramfort, A., Thirion, B., and Varoquaux, G. (2014). Machine learning for neuroimaging with scikit-learn. *Front. Neuroinform.*, 8:14.

Aglieri, V., Cagna, B., Belin, P., and Takerkart, S. (2019). Intertva. a multimodal mri dataset for the study of inter-individual differences in voice perception and identification. https://openneuro.org/datasets/ds001771/versions/1.0.2.

Bazeille, T., Richard, H., Janati, H., and Thirion, B. (2019). Local optimal transport for functional brain template estimation. In *Information Processing in Medical Imaging*, pages 237–248. Springer International Publishing.

Bellec, P., Rosa-Neto, P., Lyttelton, O. C., Benali, H., and Evans, A. C. (2010). Multi-level bootstrap analysis of stable clusters in resting-state fmri. *NeuroImage*, 51(3):1126 – 1139.

Bilenko, N. Y. and Gallant, J. L. (2016). Pyrcca: Regularized kernel canonical correlation analysis in python and its applications to neuroimaging. *Front. Neuroinform.*, 10:49.

Botvinik-Nezer, R., Holzmeister, F., Camerer, C. F., Dreber, A., Huber, J., Johannesson, M., Kirchler, M., Iwanir, R., Mumford, J. A., Adcock, R. A., et al. (2020). Variability in the analysis of a single neuroimaging dataset by many teams. *Nature*, pages 1–7.

Boyle, J. A., Pinsard, B., Boukhdhir, A., Belleville, S., Brambatti, S., Chen, J., Cohen-Adad, J., Cyr, A., Fuente, A., Rainville, P., and Bellec, P. (2020). The Courtois project on neuronal modelling: 2020 data release. https://docs.cneuromod.ca. Presented at the 26th annual meeting of the Organization for Human Brain Mapping.

Braver, T. S., Kizhner, A., Tang, R., Freund, M. C., and Etzel, J. A. (2020). The dual mechanisms of cognitive control (dmcc) project. *bioRxiv*.

Buckner, R. L., Krienen, F. M., Castellanos, A., Diaz, J. C., and Yeo, B. T. T. (2011). The organization of the human cere-

bellum estimated by intrinsic functional connectivity. *Journal of Neurophysiology*, 106(5):2322–2345. PMID: 21795627.

Chang, L. J., Gianaros, P. J., Manuck, S. B., Krishnan, A., and Wager, T. D. (2015). A sensitive and specific neural signature for Picture-Induced negative affect. *PLoS Biol.*, 13(6):e1002180.

Chang, N., Pyles, J. A., Marcus, A., Gupta, A., Tarr, M. J., and Aminoff, E. M. (2019). BOLD5000, a public fMRI dataset while viewing 5000 visual images. *Sci Data*, 6(1):49.

Chen, P.-H., Chen, J., Yeshurun, Y., Hasson, U., Haxby, J., and Ramadge, P. J. (2015). A Reduced-Dimension fMRI shared response model. In Cortes, C., Lawrence, N. D., Lee, D. D., Sugiyama, M., and Garnett, R., editors, *Advances in Neural Information Processing Systems 28*, pages 460–468. Curran Associates, Inc.

Churchland, P. M. (1998). Conceptual similarity across sensory and neural diversity: the Fodor/Lepore challenge answered. *J. Philos.*, 95(1):5–32.

Cuturi, M. (2013). Sinkhorn distances: Lightspeed computation of optimal transport. In Burges, C. J. C., Bottou, L., Welling, M., Ghahramani, Z., and Weinberger, K. Q., editors, *Advances in Neural Information Processing Systems 26*, pages 2292–2300. Curran Associates, Inc.

Dockès, J., Poldrack, R. A., Primet, R., Gözükan, H., Yarkoni, T., Suchanek, F., Thirion, B., and Varoquaux, G. (2020). Neuroquery, comprehensive meta-analysis of human brain mapping. *eLife*, 9:e53385.

Esteban, O., Markiewicz, C. J., Blair, R. W., Moodie, C. A., Isik, A. I., Erramuzpe, A., Kent, J. D., Goncalves, M., DuPre, E., Snyder, M., Oya, H., Ghosh, S. S., Wright, J., Durnez, J., Poldrack, R. A., and Gorgolewski, K. J. (2019). fMRIPrep: a robust preprocessing pipeline for functional MRI. *Nat. Methods*, 16(1):111–116.

Güçlü, U. and van Gerven, M. A. (2015). Deep neural networks reveal a gradient in the complexity of neural representations across the ventral stream. *Journal of Neuroscience*, 35(27):10005–10014.

Guntupalli, J. S., Feilong, M., and Haxby, J. V. (2018). A computational model of shared fine-scale structure in the human connectome. *PLoS Comput. Biol.*, 14(4):e1006120.

Guntupalli, J. S., Hanke, M., Halchenko, Y. O., Connolly, A. C., Ramadge, P. J., and Haxby, J. V. (2016). A model of representational spaces in human cortex. *Cereb. Cortex*, 26(6):2919–2934.

Hanke, M., Adelhöfer, N., Kottke, D., Iacovella, V., Sengupta, A., Kaule, F. R., Nigbur, R., Waite, A. Q., Baumgartner, F., and Stadler, J. (2016). A studyforrest extension, simultaneous fMRI and eye gaze recordings during prolonged natural stimulation. *Sci Data*, 3:160092.

Hanke, M., Halchenko, Y. O., Sederberg, P. B., Hanson, S. J., Haxby, J. V., and Pollmann, S. (2009). PyMVPA: A python toolbox for multivariate pattern analysis of fMRI data. *Neuroinformatics*, 7(1):37–53.

Haxby, J. V., Guntupalli, J. S., Connolly, A. C., Halchenko, Y. O., Conroy, B. R., Gobbini, M. I., Hanke, M., and Ramadge, P. J. (2011). A common, high-dimensional model of the representational space in human ventral temporal cortex. *Neuron*, 72(2):404–416.

Haxby, J. V., Guntupalli, J. S., Nastase, S. A., and Feilong, M. (2020). Hyperalignment: Modeling shared information encoded in idiosyncratic cortical topographies. *Elife*, 9:e56601.

Heller, R., Golland, Y., Malach, R., and Benjamini, Y. (2007). Conjunction group analysis: An alternative to mixed/random effect analysis. *NeuroImage*, 37:1178–85.

Jiahui, G., Feilong, M., Visconti di Oleggio Castello, M., Guntupalli, J. S., Chauhan, V., Haxby, J. V., and Gobbini, M. I. (2020). Predicting individual face-selective topography using naturalistic stimuli. *Neuroimage*, 216:116458.

Kriegeskorte, N. and Diedrichsen, J. (2019). Peeling the onion of brain representations. *Annu. Rev. Neurosci.*, 42(1):407–432.

Kriegeskorte, N., Goebel, R., and Bandettini, P. (2006). Information-based functional brain mapping. *Proc. Natl. Acad. Sci. U. S. A.*, 103(10):3863–3868.

Langs, G., Golland, P., Tie, Y., Rigolo, L., and Golby, A. J. (2010). Functional geometry alignment and localization of brain areas. *Adv. Neural Inf. Process. Syst.*, 1:1225–1233.

Langs, G., Sweet, A., Lashkari, D., Tie, Y., Rigolo, L., Golby, A. J., and Golland, P. (2014). Decoupling function and anatomy in atlases of functional connectivity patterns: language mapping in tumor patients. *Neuroimage*, 103:462–475.

Nastase, S. A., Gazzola, V., Hasson, U., and Keysers, C. (2019). Measuring shared responses across subjects using intersubject correlation.

Olivetti, E., Veeramachaneni, S., and Avesani, P. (2011). Testing for information with brain decoding. In *2011 International Workshop on Pattern Recognition in NeuroImaging*, pages 33–36.

Oosterhof, N. N., Wiestler, T., Downing, P. E., and Diedrichsen, J. (2011). A comparison of volume-based and surface-based multi-voxel pattern analysis. *Neuroimage*, 56(2):593–600.

O'Connor, D., Potler, N. V., Kovacs, M., Xu, T., Ai, L., Pellman, J., Vanderwal, T., Parra, L. C., Cohen, S., Ghosh, S., et al. (2017). The healthy brain network serial scanning initiative: a resource for evaluating inter-individual differences and their reliabilities across scan conditions and sessions. *Gigascience*, 6(2):giw011.

Paquola, C., De Wael, R. V., Wagstyl, K., Bethlehem, R. A., Hong, S.-J., Seidlitz, J., Bullmore, E. T., Evans, A. C., Misic, B., Margulies, D. S., et al. (2019). Microstructural and functional gradients are increasingly dissociated in transmodal cortices. *PLOS Biology*, 17(5):e3000284.

Pedregosa, F., Varoquaux, G., Gramfort, A., Michel, V., Thirion, B., Grisel, O., Blondel, M., Prettenhofer, P., Weiss, R., Dubourg, V., Vanderplas, J., Passos, A., Cournapeau, D., Brucher, M., Perrot, M., and Duchesnay, E. (2011). Scikit-learn: Machine learning in Python. *Journal of Machine Learning Research*, 12:2825–2830.

Pinho, A. L., Amadon, A., Ruest, T., Fabre, M., Dohmatob, E., Denghien, I., Ginisty, C., Becuwe-Desmidt, S., Roger, S., Laurier, L., Joly-Testault, V., Médiouni-Cloarec, G., Doublé,

C., Martins, B., Pinel, P., Eger, E., Varoquaux, G., Pallier, C., Dehaene, S., Hertz-Pannier, L., and Thirion, B. (2018). Individual brain charting, a high-resolution fMRI dataset for cognitive mapping. *Sci Data*, 5:180105.

Poldrack, R. A., Barch, D. M., Mitchell, J., Wager, T., Wagner, A. D., Devlin, J. T., Cumba, C., Koyejo, O., and Milham, M. (2013). Toward open sharing of task-based fmri data: the openfmri project. *Frontiers in neuroinformatics*, 7:12.

Rademacher, J., Caviness, Jr, V. S., Steinmetz, H., and Galaburda, A. M. (1993). Topographical variation of the human primary cortices: implications for neuroimaging, brain mapping, and neurobiology. *Cereb. Cortex*, 3(4):313–329.

Richard, H., Martin, L., Pinho, A. L., Pillow, J., and Thirion, B. (2019). Fast shared response model for fmri data. *arXiv preprint arXiv:1909.12537*.

Rodriguez-Vazquez, B., Suarez, L. E., Shafiei, G., Markello, R., Paquola, C., Hagmann, P., Van Den Heuvel, M., Bernhardt, B., Spreng, R. N., and Misic, B. (2019). Gradients of structure-function tethering across neocortex. *BioRxiv*, page 561985.

Sabuncu, M., Bryan, E., Ramadge, P. J., and Haxby, J. V. (2010). Function-based intersubject alignment of human cortical anatomy. *Cerebral Cortex*, 20:130–140.

Schaefer, A., Kong, R., Gordon, E. M., Laumann, T. O., Zuo, X.-N., Holmes, A. J., Eickhoff, S. B., and Yeo, B. T. T. (2018). Local-Global parcellation of the human cerebral cortex from intrinsic functional connectivity MRI. *Cereb. Cortex*, 28(9):3095–3114.

Schrouff, J., Monteiro, J. M., Portugal, L., Rosa, M. J., Phillips, C., and Mourao-Miranda, J. (2018). Embedding Anatomical or Functional Knowledge in Whole-Brain Multiple Kernel Learning Models. *Neuroinformatics*, 16(1):117–143.

Tavor, I., Parker Jones, O., Mars, R. B., Smith, S. M., Behrens, T. E., and Jbabdi, S. (2016). Task-free MRI predicts individual differences in brain activity during task performance. *Science*, 352(6282):216–220.

Thirion, B., Flandin, G., Pinel, P., Roche, A., Ciuciu, P., and Poline, J.-B. (2006). Dealing with the shortcomings of spatial normalization: multi-subject parcellation of fMRI datasets. *Hum. Brain Mapp.*, 27(8):678–693.

Varoquaux, G., Gramfort, A., Pedregosa, F., Michel, V., and Thirion, B. (2011). Multi-subject dictionary learning to segment an atlas of brain spontaneous activity. In *Information Processing in Medical Imaging*, volume 6801 of *Lecture Notes in Computer Science*, pages 562–573, Kaufbeuren, Germany. Gábor Székely, Horst Hahn, Springer.

Virtanen, P., Gommers, R., Oliphant, T. E., Haberland, M., Reddy, T., Cournapeau, D., Burovski, E., Peterson, P., Weckesser, W., Bright, J., et al. (2020). Scipy 1.0: fundamental algorithms for scientific computing in python. *Nature methods*, 17(3):261–272.

Xu, T., Yousefnezhad, M., and Zhang, D. (2018). Gradient hyperalignment for multi-subject fmri data alignment. In *Pacific Rim International Conference on Artificial Intelligence*, pages 1058–1068. Springer.

Yousefnezhad, M. and Zhang, D. (2017). Deep hyperalignment. In Guyon, I., Luxburg, U. V., Bengio, S., Wallach, H., Fergus, R., Vishwanathan, S., and Garnett, R., editors, *Advances in Neural Information Processing Systems 30*, pages 1604–1612. Curran Associates, Inc.

An empirical evaluation of functional alignment using inter-subject decoding

Thomas Bazeille†, Elizabeth DuPre†, Jean-Baptiste Poline, and Bertrand Thirion
†*These authors contributed equally to this work.*

SUPPLEMENTAL MATERIALS

S1. FMRIPREP PREPROCESSING

Results included in this manuscript come from preprocessing performed using *fMRIPrep* 20.1.1+38.g8480eabb (Esteban et al. 2018b; Esteban et al. 2018a; RRID:SCR_016216), which is based on *Nipype* 1.5.0 (Gorgolewski et al. 2011; Gorgolewski et al. 2018; RRID:SCR_002502).

S1.1. Anatomical data preprocessing

The T1-weighted (T1w) image was corrected for intensity non-uniformity (INU) with N4BiasFieldCorrection (Tustison et al. 2010), distributed with ANTs 2.2.0 (Avants et al. 2008, RRID:SCR_004757), and used as T1w-reference throughout the workflow. The T1w-reference was then skull-stripped with a Nipype implementation of the antsBrainExtraction.sh workflow (from ANTs), using OASIS30ANTs as target template. Brain tissue segmentation of cerebrospinal fluid (CSF), white-matter (WM) and gray-matter (GM) was performed on the brain-extracted T1w using fast (FSL 5.0.9, RRID:SCR_002823, Zhang et al. 2001). Volume-based spatial normalization to one standard space (MNI152NLin2009cAsym) was performed through nonlinear registration with antsRegistration (ANTs 2.2.0), using brain-extracted versions of both T1w reference and the T1w template. The following template was selected for spatial normalization: ICBM 152 Nonlinear Asymmetrical template version 2009c (Fonov et al. 2009, RRID:SCR_008796; TemplateFlow ID: MNI152NLin2009cAsym).

S1.2. Functional data preprocessing

For each subject's BOLD runs (across all tasks and sessions), the following preprocessing was performed. First, a reference volume and its skull-stripped version were generated by aligning and averaging 1 single-band references (SBRefs). A B0-nonuniformity map (or *fieldmap*) was estimated based on two (or more) echo-planar imaging (EPI) references with opposing phase-encoding directions, with `3dQwarp` Cox and Hyde (1997) (AFNI 20160207). Based on the estimated susceptibility distortion, a corrected EPI (echo-planar imaging) reference was calculated for a more accurate co-registration with the anatomical reference. The BOLD reference was then co-registered to the T1w reference using `bbregister` (FreeSurfer) which implements boundary-based registration (Greve and Fischl 2009). Co-registration was configured with six degrees of freedom. Head-motion parameters with respect to the BOLD reference (transformation matrices, and six corresponding rotation and translation parameters) are estimated before any spatiotemporal filtering using `mcflirt` (FSL 5.0.9, Jenkinson et al. 2002).

First, a reference volume and its skull-stripped version were generated using a custom methodology of *fMRIPrep*. The BOLD time-series (including slice-timing correction when applied) were resampled onto their original, native space by applying a single, composite transform to correct for head-motion and susceptibility distortions. These resampled BOLD time-series will be referred to as *preprocessed BOLD in original space*, or just *preprocessed BOLD*. The BOLD time-series were resampled into standard space, generating a *preprocessed BOLD run in MNI152NLin2009cAsym space*. First, a reference volume and its skull-stripped version were generated using a custom methodology of *fMRIPrep*.

All resamplings can be performed with *a single interpolation step* by composing all the pertinent transformations (i.e. head-motion transform matrices, susceptibility distortion correction when available, and co-registrations to anatomical and output spaces). Gridded (volumetric) resamplings were performed using `antsApplyTransforms` (ANTs), configured with Lanczos interpolation to minimize the smoothing effects of other kernels (Lanczos 1964).

Many internal operations of *fMRIPrep* use *Nilearn* 0.6.2 (Abraham et al. 2014, RRID:SCR_001362), mostly within the functional processing workflow. For more details of the pipeline, see the section corresponding to workflows in *fMRIPrep*'s documentation.

S1.3. Copyright Waiver

S2. ABSOLUTE DECODING ACCURACY OF VARIOUS METHODS

Tables S1 and S2 report absolute decoding accuracies for *Experiment 1* and *Experiment 2*, to bring a different view of results presented in Figures 5 and 7, as relative improvements brought over anatomical registration by various alignment methods. This "per dataset view" highlight that gains brought by best methods are substantial improvement over baseline, especially when compared to chance.

S3. WHOLE-BRAIN DECODING PROVIDES BETTER ACCURACY THAN ROI-BASED DECODING

In Figure S1, we compare ROI-based and whole-brain inter-subject decoding accuracy improvements for piecewise Procrustes alignment above anatomical-only alignment. We see that whole-brain alignment generally shows higher inter-subject decoding improvements compared to ROI-based alignment. As mentioned in the main text, this result supports previous work from the inter-subject decoding literature (Chang et al. 2015, Schrouff et al. 2018), and it suggests that full-brain piecewise alignment yields the best overall decoding pipeline.

S4. PARCELLATION HAS LIMITED IMPACT ON DECODING ACCURACY

To assess the impact of the parcellation used on piecewise alignment results, we compared decoding accuracy gains while varying the parcellation kind and resolution. First, we consider the multi-resolution Schaefer et al. (2018) atlas, which was learnt using a gradient weighted markov random field on resting state data from 1489 subjects. We compare this *a priori* parcellation to two parcellations learnt directly on the subject's alignment data after 5mm FWHM Gaussian smoothing: K-means or Hierarchical K-means. All these parcellations were taken at ten resolutions from 100 to 1000 parcels.

As hierarchical K-means may be less familiar to readers, we briefly describe it in more detail here. This method is a variant of K-means aimed specifically at obtaining more balanced parcels. To identify k parcels, we first apply K-means to cluster the voxels in $\sqrt{k}$ big clusters. Each of these "big clusters" is then clustered again in $\sqrt{k}$ to obtain a total of k smaller well-balanced parcels. In this experiment, K-means and Hierarchical K-means implementations used are respectively from `scikit-learn` and `fmralign`, and fitted as part of `fmralign` alignment functions on the source subject data.

We plot piecewise Procustes accuracy improvements for these three parcellation methods and ten resolutions in Figure S2. Here, we only show the IBC Sounds and IBC RSVP decoding tasks to ease in interpretation. Overall, we observe on these two tasks that the type and resolution of parcellation used does not have a strong impact on accuracy improvements above anatomical-only alignment. We therefore suggest that *piecewise alignment* can be used with confidence that the parcellation choice won't strongly impact its results.

S5. FUNCTIONAL ALIGNMENT IS NOT MERELY SMOOTHING

Gaussian smoothing is a common preprocessing step in neuroimaging group studies, which reconciles dissimilar subject-level signals by smoothing over inter-individual variability. Our qualitative results (section 3.3) show that best performing alignment methods do not seem to smooth the signal across voxels, but instead preserve the signal specificity while matching its geometry with the target subject functional topography. Nonetheless, since both of these techniques aim to reconcile inter-individual variability, we aimed to directly compare Gaussian smoothing and functional alignment in a control analysis. Specifically, we compared decoding gains from six different Gaussian smoothing kernels to those obtained through the reference method piecewise Procrustes alignment.

The results displayed in Figure S3 clearly support previous findings (Guntupalli et al. 2016) that smoothing does not improve inter-subject decoding performance—and therefore recover mutual information—in the same way that functional alignment.

S6. IMPACT OF THE DATA REPRESENTATION AND RESOLUTION

Oosterhof et al. 2011 argued that functional alignment benefits from working with a representation of the fMRI signal on the cortical surface (Coalson et al. 2018). Relatedly, we would also expect that the resolution of the data representation—whether in the surface or the volume—will impact the quality of the alignment learnt.

To assess the dependence of our 3mm volumetric results presented in the main text on sampling parameters, we replicated our inter-subject decoding framework with the IBC RSVP language task data on a high-resolution cortical surface representation(*fsaverage7*)(obtained through `freesurfer` surfacic projection of full-resolution raw images in their respective subject space, later on mapped to the common surfacic template). This surface mesh includes 168k cortical nodes per hemisphere, which we divided into 350 parcels per hemisphere using *Schaefer* atlas at scale 700.

We provide results for the inter-subject decoding accuracy gains seen with the reference functional alignment method of piecewise Procrustes over standard, anatomical-only alignment. We had to limit to this setting because (i) replicating this analysis on every dataset

Methods/Dataset	IBC RSVP	IBC Sounds	Forrest	BOLD5000	Neuromod
Chance	16.7	16.7	20	25.5	25
Anatomical	38.2 ± 0.2	32.7 ± 0.3	31.4 ± 0.2	33.3 ± 0.1	**72.1** ± 6.5
Intra-subject	39.6 ± 0.1	36.4 ± 0.8	32.3 ± 0.3	35.1 ± 0.1	69.7 ± 2.3
Searchlight Procrustes	38.5 ± 0.4	32.3 ± 0.7	31.5 ± 0.2	35.2 ± 0.1	67.3 ± 3.4
Piecewise Procrustes	42.0 ± 0.2	36.6 ± 0.3	33.3 ± 0.2	**38.5** ± 0.1	66.3 ± 5.2
Piecewise Optimal Transport	**43.5** ± 0.3	**38.1** ± 1.0	**33.5** ± 0.2	38.1 ± 0.1	71.6 ± 6.4
Shared Response Model	27.1 ± 0.2	25.8 ± 0.5	28.8 ± 0.1	37.2 ± 0.2	37.0 ± 0.4

TABLE S1. **Fullbrain benchmark absolute decoding accuracy** (%)

Methods/Dataset	IBC RSVP	IBC Sounds	Forrest	BOLD5000	Neuromod
Chance	16.7	16.7	20	25.5	25
Anatomical	22.2 ± 0.1	26.8 ± 0.5	30.8 ± 0.4	33.8 ± 0.1	64.9 ± 0.5
Intra-subject	22.0 ± 0.0	25.6 ± 0.1	29.2 ± 0.4	34.2 ± 0.1	**65.5** ± 1.9
Searchlight Procrustes	27.8 ± 0.1	25.9 ± 0.2	29.8 ± 0.5	34.1 ± 0.1	57.2 ± 5.0
Piecewise Procrustes	24.0 ± 0.0	24.2 ± 0.7	28.5 ± 0.2	39.6 ± 0.1	56.7 ± 4.9
Piecewise Optimal Transport	25.9 ± 0.1	24.6 ± 0.3	28.5 ± 0.2	39.6 ± 0.1	65.4 ± 2.4
Shared Response Model	**30.6** ± 0.2	**31.0** ± 0.5	**35.8** ± 0.4	**40.9** ± 0.1	38.5 ± 0.8

TABLE S2. **ROI benchmark absolute decoding accuracy** (%)

would represent an important amount of processing work, and (ii) working on other methods than piecewise Procrustes on this very large data is computationally prohibitive.

The results displayed in Figure S4 show that although decoding gains are a little higher using high-resolution surface-based representation, they remain in the same range as the volume-based representation. This shows that a 10-fold higher resolution can help match more precisely topographies across subjects (and reduce the decoding variance as a consequence), but no important marginal gains can be expected from it. In the end the signal available for use is bounded by the same rough limitations: test-retest reliability in each subject.

Abraham, A., Pedregosa, F., Eickenberg, M., Gervais, P., Mueller, A., Kossaifi, J., Gramfort, A., Thirion, B., and Varoquaux, G. (2014). Machine learning for neuroimaging with scikit-learn. *Frontiers in Neuroinformatics*, 8.

Avants, B., Epstein, C., Grossman, M., and Gee, J. (2008). Symmetric diffeomorphic image registration with cross-correlation: Evaluating automated labeling of elderly and neurodegenerative brain. *Medical Image Analysis*, 12(1):26–41.

Chang, L. J., Gianaros, P. J., Manuck, S. B., Krishnan, A., and Wager, T. D. (2015). A sensitive and specific neural signature for Picture-Induced negative affect. *PLoS Biol.*, 13(6):e1002180.

Coalson, T. S., Van Essen, D. C., and Glasser, M. F. (2018). The impact of traditional neuroimaging methods on the spatial localization of cortical areas. *Proceedings of the National Academy of Sciences*, 115(27):E6356–E6365.

Cox, R. W. and Hyde, J. S. (1997). Software tools for analysis and visualization of fmri data. *NMR in Biomedicine*, 10(4-5):171–178.

Esteban, O., Blair, R., Markiewicz, C. J., Berleant, S. L., Moodie, C., Ma, F., Isik, A. I., Erramuzpe, A., Kent, James D. andGoncalves, M., DuPre, E., Sitek, K. R., Gomez, D. E. P., Lurie, D. J., Ye, Z., Poldrack, R. A., and Gorgolewski, K. J. (2018a). fmriprep. *Software*.

Esteban, O., Markiewicz, C., Blair, R. W., Moodie, C., Isik, A. I., Erramuzpe Aliaga, A., Kent, J., Goncalves, M., DuPre, E., Snyder, M., Oya, H., Ghosh, S., Wright, J., Durnez, J., Poldrack, R., and Gorgolewski, K. J. (2018b). fMRIPrep: a robust preprocessing pipeline for functional MRI. *Nature Methods*.

Fonov, V., Evans, A., McKinstry, R., Almli, C., and Collins, D. (2009). Unbiased nonlinear average age-appropriate brain templates from birth to adulthood. *NeuroImage*, 47, Supplement 1:S102.

Gorgolewski, K., Burns, C. D., Madison, C., Clark, D., Halchenko, Y. O., Waskom, M. L., and Ghosh, S. (2011). Nipype: a flexible, lightweight and extensible neuroimaging data processing framework in python. *Frontiers in Neuroinformatics*, 5:13.

Gorgolewski, K. J., Esteban, O., Markiewicz, C. J., Ziegler, E., Ellis, D. G., Notter, M. P., Jarecka, D., Johnson, H., Burns, C., Manhães-Savio, A., Hamalainen, C., Yvernault, B., Salo, T., Jordan, K., Goncalves, M., Waskom, M., Clark, D., Wong, J., Loney, F., Modat, M., Dewey, B. E., Madison,

C., Visconti di Oleggio Castello, M., Clark, M. G., Dayan, M., Clark, D., Keshavan, A., Pinsard, B., Gramfort, A., Berleant, S., Nielson, D. M., Bougacha, S., Varoquaux, G., Cipollini, B., Markello, R., Rokem, A., Moloney, B., Halchenko, Y. O., Wassermann, D., Hanke, M., Horea, C., Kaczmarzyk, J., de Hollander, G., DuPre, E., Gillman, A., Mordom, D., Buchanan, C., Tungaraza, R., Pauli, W. M., Iqbal, S., Sikka, S., Mancini, M., Schwartz, Y., Malone, I. B., Dubois, M., Frohlich, C., Welch, D., Forbes, J., Kent, J., Watanabe, A., Cumba, C., Huntenburg, J. M., Kastman, E., Nichols, B. N., Eshaghi, A., Ginsburg, D., Schaefer, A., Acland, B., Giavasis, S., Kleesiek, J., Erickson, D., Küttner, R., Haselgrove, C., Correa, C., Ghayoor, A., Liem, F., Millman, J., Haehn, D., Lai, J., Zhou, D., Blair, R., Glatard, T., Renfro, M., Liu, S., Kahn, A. E., Pérez-García, F., Triplett, W., Lampe, L., Stadler, J., Kong, X.-Z., Hallquist, M., Chetverikov, A., Salvatore, J., Park, A., Poldrack, R., Craddock, R. C., Inati, S., Hinds, O., Cooper, G., Perkins, L. N., Marina, A., Mattfeld, A., Noel, M., Snoek, L., Matsubara, K., Cheung, B., Rothmei, S., Urchs, S., Durnez, J., Mertz, F., Geisler, D., Floren, A., Gerhard, S., Sharp, P., Molina-Romero, M., Weinstein, A., Broderick, W., Saase, V., Andberg, S. K., Harms, R., Schlamp, K., Arias, J., Papadopoulos Orfanos, D., Tarbert, C., Tambini, A., De La Vega, A., Nickson, T., Brett, M., Falkiewicz, M., Podranski, K., Linkersdörfer, J., Flandin, G., Ort, E., Shachnev, D., McNamee, D., Davison, A., Varada, J., Schwabacher, I., Pellman, J., Perez-Guevara, M., Khanuja, R., Pannetier, N., McDermottroe, C., and Ghosh, S. (2018). Nipype. *Software*.

Greve, D. N. and Fischl, B. (2009). Accurate and robust brain image alignment using boundary-based registration. *NeuroImage*, 48(1):63–72.

Guntupalli, J. S., Hanke, M., Halchenko, Y. O., Connolly, A. C., Ramadge, P. J., and Haxby, J. V. (2016). A model of representational spaces in human cortex. *Cereb. Cortex*, 26(6):2919–2934.

Jenkinson, M., Bannister, P., Brady, M., and Smith, S. (2002). Improved optimization for the robust and accurate linear registration and motion correction of brain images. *NeuroImage*, 17(2):825–841.

Lanczos, C. (1964). Evaluation of noisy data. *Journal of the Society for Industrial and Applied Mathematics Series B Numerical Analysis*, 1(1):76–85.

Oosterhof, N. N., Wiestler, T., Downing, P. E., and Diedrichsen, J. (2011). A comparison of volume-based and surface-based multi-voxel pattern analysis. *Neuroimage*, 56(2):593–600.

Schaefer, A., Kong, R., Gordon, E. M., Laumann, T. O., Zuo, X.-N., Holmes, A. J., Eickhoff, S. B., and Yeo, B. T. T. (2018). Local-Global parcellation of the human cerebral cortex from intrinsic functional connectivity MRI. *Cereb. Cortex*, 28(9):3095–3114.

Schrouff, J., Monteiro, J. M., Portugal, L., Rosa, M. J., Phillips, C., and Mourao-Miranda, J. (2018). Embedding Anatomical or Functional Knowledge in Whole-Brain Multiple Kernel Learning Models. *Neuroinformatics*, 16(1):117–143.

Tustison, N. J., Avants, B. B., Cook, P. A., Zheng, Y., Egan, A., Yushkevich, P. A., and Gee, J. C. (2010). N4itk: Improved n3 bias correction. *IEEE Transactions on Medical Imaging*, 29(6):1310–1320.

Zhang, Y., Brady, M., and Smith, S. (2001). Segmentation of brain MR images through a hidden markov random field model and the expectation-maximization algorithm. *IEEE Transactions on Medical Imaging*, 20(1):45–57.

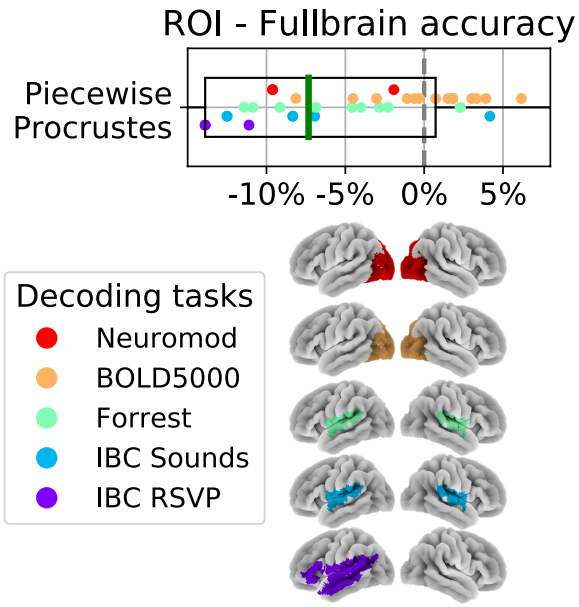

FIG. S1. **Comparing ROI and whole-brain decoding accuracy after piecewise Procrustes alignment.** The ROIs used for each dataset are displayed on the *lower panel*. In the *upper panel*, we show the distribution of differences in decoding accuracy scores between ROI-based and whole-brain piecewise Procrustes alignment. Each dot represents a single subject, and subjects are colored according to their decoding task. Each difference score is calculated by subtracting the inter-subject decoding accuracy for whole-brain piecewise Procrustes alignment from the ROI-based piecewise Procrustes alignment accuracy scor—for the same leave-one-subject-out cross-validation fold. The box plot thus describes the distribution of differences, where the green line represents the median value. We see that decoding accuracy is lower when performed within ROIs than when performed on the whole-brain data.

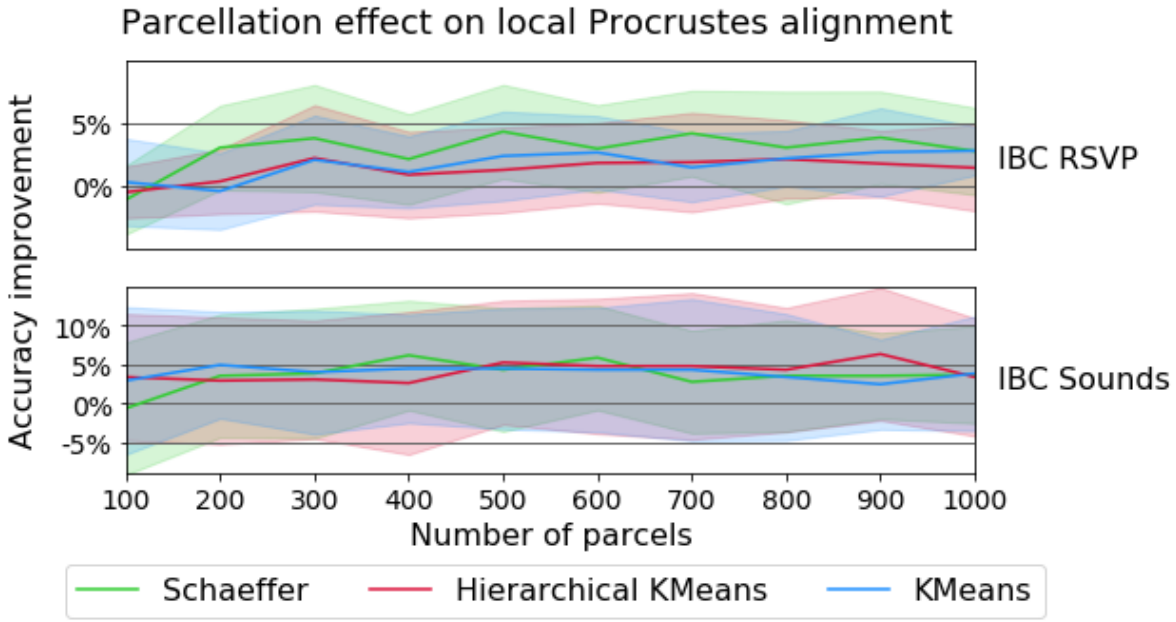

FIG. S2. **Effect of parcellation type, resolution on Piecewise Procrustes decoding accuracy improvement over anatomical alignment.** We consider the impact of parcellation type (the *a priori* Schaefer atlas or learned directly on the data with k-means or hierarchical k-means) and resolution (from 100 to 1000 parcels). Results are shown for the IBC RSVP and IBC Sounds decoding tasks. Each line represents the average accuracy improvement for piecewise Procruses over standard, anatomical-only alignment, and the confidence band represents the range of accuracy improvements seen across all IBC subjects. Accuracy improvements are calculated by subtracting anatomical-only inter-subject decoding accuracy scores for the same leave-one-subject-out cross-validation fold. We see that parcellation type and resolution show limited impact on accuracy gains.

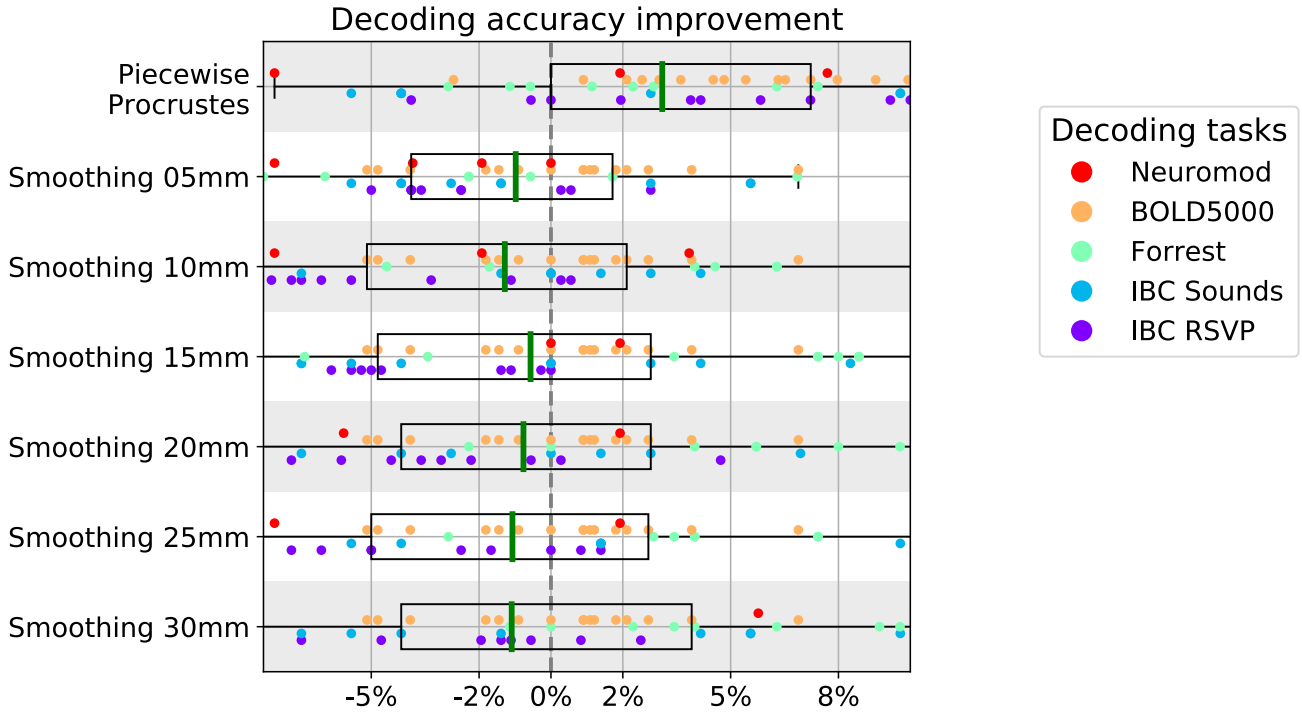

FIG. S3. **Decoding accuracy does not improve after Gaussian smoothing over anatomical alignment.** For six smoothing kernels, we show inter-subject decoding accuracy scores after subtracting anatomical-only inter-subject decoding accuracy for the same leave-one-subject-out cross-validation fold. Each dot represents a single subject, and subjects are colored according to their decoding task. We also show differences in decoding accuracy scores for the reference functional alignment method piecewise Procrustes, again as compared to anatomical-only alignment. Each box plot describes the distribution of values for that smoothing kernel or alignment method, and the green line indicates the median. We see that Gaussian smoothing does not show the same pattern of decoding accuracy differences as the reference functional alignment method.

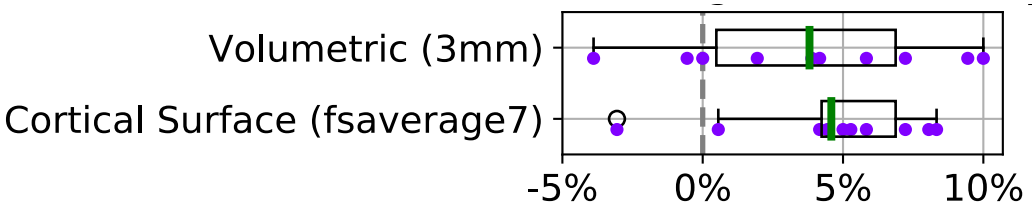

FIG. S4. **Comparing piecewise Procrustes accuracy improvements across volumetric and surface data representations.** For the IBC RSVP task, we compare piecewise Procrustes decoding accuracy scores to anatomical-only alignment. Each dot represents an IBC subject, where their difference score is calculated by subtracting the inter-subject decoding accuracy for anatomical-only alignment from the piecewise Procrustes alignment accuracy score for the same leave-one-subject-out cross-validation fold; i.e., where they are the left-out subject. We compare these difference scores as calculated using data in the volume (3mm resolution), to data on the high-resolution cortical surface (*fsaverage7*). Each box plot describes the distribution of values for that data representation, and the green line indicates the median. We see that the high-resolution surface representation yields a moderate gain of decoding accuracy, compared to 3mm isotropic volumetric representation.